
This is an electronic reprint of the original article.
This reprint may differ from the original in pagination and typographic detail.

Bandemehr, Jascha; Zimmerhofer, Fabian; Ivlev, Sergei I.; Pietzonka, Clemens; Eklund, Kim; Karttunen, Antti J.; Huppertz, Hubert; Kraus, Florian

Syntheses and Characterization of the Mixed-Valent Manganese(II/III) Fluorides Mn_2F_5 and Mn_3F_8

Published in:
Inorganic Chemistry

DOI:
[10.1021/acs.inorgchem.1c01833](https://doi.org/10.1021/acs.inorgchem.1c01833)

Published: 06/09/2021

Document Version
Peer-reviewed accepted author manuscript, also known as Final accepted manuscript or Post-print

Published under the following license:
Unspecified

Please cite the original version:
Bandemehr, J., Zimmerhofer, F., Ivlev, S. I., Pietzonka, C., Eklund, K., Karttunen, A. J., Huppertz, H., & Kraus, F. (2021). Syntheses and Characterization of the Mixed-Valent Manganese(II/III) Fluorides Mn_2F_5 and Mn_3F_8 . *Inorganic Chemistry*, 60(17), 12651-12663. <https://doi.org/10.1021/acs.inorgchem.1c01833>

This material is protected by copyright and other intellectual property rights, and duplication or sale of all or part of any of the repository collections is not permitted, except that material may be duplicated by you for your research use or educational purposes in electronic or print form. You must obtain permission for any other use. Electronic or print copies may not be offered, whether for sale or otherwise to anyone who is not an authorised user.

Syntheses and Characterization of the Mixed-Valent Mn(II/III) Fluorides Mn₂F₅ and Mn₃F₈

Jascha Bandemehr^{a, §}, Fabian Zimmerhofer^{b, §}, Sergei I. Ivlev^a, Clemens Pietzonka^a, Kim Eklund,^c Antti J. Karttunen,^c Hubert Huppertz^b, Florian Kraus^{a*}

^a M. Sc. Jascha Bandemehr, Dr. (RUS) Sergei I. Ivlev, C. Pietzonka, Prof. Dr. Florian Kraus, Fachbereich Chemie, Philipps-Universität Marburg, Hans-Meerwein-Str. 4, 35032 Marburg, Germany, f.kraus@uni-marburg.de

^b M. Sc. Fabian Zimmerhofer, Univ.-Prof. Dr. H. Huppertz, Institut für Allgemeine, Anorganische und Theoretische Chemie, Universität Innsbruck, Innrain 80-82, 6020 Innsbruck, Austria

^c M. Sc. Kim Eklund, Prof. Dr. Antti Karttunen, Department of Chemistry and Materials Science, Aalto University 00076 Aalto, Finland

[§] J. Bandemehr and F. Zimmerhofer contributed equally to this work.

Abstract

We obtained single crystals of the binary mixed-valent fluorides Mn₂F₅ and Mn₃F₈ using a high-pressure/high-temperature approach. Mn₂F₅ crystallizes isotypic to CaCrF₅ in the monoclinic space group *C2/c* (no. 15), with $a = 8.7078(8)$, $b = 6.1473(6)$, $c = 7.7817(7)$ Å, $\beta = 117.41(1)^\circ$, $V = 369.80(6)$ Å³, $Z = 4$, *mC28*, at $T = 173$ K. Mn₃F₈ crystallizes in the monoclinic space group *P2₁* (no. 4) with $a = 5.5253(2)$, $b = 4.8786(2)$, $c = 9.9124(4)$ Å, $\beta = 92.608(2)^\circ$, $V = 266.92(2)$ Å³, $Z = 2$, *mP22*, at $T = 183$ K, and presents a new structure type. Crystal-chemical reasoning, CHARDI calculations, and quantum chemical calculations allowed for the assignment of the oxidation states of the Mn atoms. In both bulk compounds MnF₂ was present as an impurity, as evidenced by powder X-ray diffraction and IR and Raman spectroscopy.

Keywords

Manganese; fluoride; crystal structure; magnetism; spectroscopy; quantum chemical calculations

Introduction

The first discovered fluoride of manganese was MnF_2 . The pale pink compound is well characterized and its crystal structure is isotypic to MgF_2 (rutile type).^{1,2} It can be synthesized by carefully adding MnCO_3 to hydrofluoric acid.¹

MnF_3 is a hygroscopic, ruby red compound, which was first mentioned in 1867,³ however the first proof that pure MnF_3 was synthesized was finally given in 1900 by *Moissan*.⁴ MnF_3 can be prepared by fluorination of MnF_2 or MnI_2 at 250 °C, or by thermal decomposition of $(\text{NH}_4)_2\text{MnF}_5$ at 250 °C in a stream of fluorine.⁴⁻⁶ In anhydrous HF as a solvent, the oxidation of MnF_2 with F_2 to MnF_3 proceeds already at room temperature.⁷ Its crystal structure was first described in 1957,^{8,9} redetermined in 1993,¹⁰ and finally corrected in 2020.¹¹

MnF_4 was first described by Hoppe and co-workers. The blue compound is more hygroscopic than MnF_3 .^{12,13} It can be synthesized by direct fluorination of Mn above 300 °C,^{13,14} by Lewis acid-base reaction of e.g. AsF_5 with $[\text{MnF}_6]^{2-}$ anions in anhydrous HF,¹⁵ by thermal decomposition of $\text{KrF}_2 \cdot \text{MnF}_4$ or $2\text{KrF}_2 \cdot \text{MnF}_4$,¹⁶ or photochemically from a mixture of MnF_3 and F_2 in anhydrous HF.⁷ Two polymorphs of MnF_4 are known. α - MnF_4 crystallizes in space group $I4/a$ (no. 88) with $Z = 16$,¹⁷ and β - MnF_4 crystallizes in space group $R3c$ (no. 161) with $Z = 72$.¹⁸

Besides these di-, tri- and tetravalent fluorides the mixed-valent manganese(II/III) fluoride Mn_2F_5 was suggested to form during partial decomposition of MnF_3 ,¹⁹ and was later obtained as a powder by *Tressaud* and *Dance* in the year 1974 by heating a mixture of MnF_2 and MnF_3 in a gold ampoule up to 300 °C.²⁰ The lattice parameters were reported as $a = (15.44 \pm 0.02)$, $b = (7.27 \pm 0.01)$, $c = (6.17 \pm 0.01)$ Å, $V \approx 693$ Å³ in the orthorhombic crystal system, and the authors suspected that the structure should be related to MnCrF_5 and those of other transition metal fluorides of the composition ABF_5 with A and B being divalent and trivalent transition metals, respectively. MnCrF_5 had been reported orthorhombic, space group $Cmmm$ in 1971,²¹ and was corrected in 1978 to be monoclinic, space group $C2/c$.²² *Tressaud* and *Dance* concluded that the Mn(II) atoms should show a distorted octahedral coordination sphere, while corner-sharing $[\text{MnF}_6]^{3-}$ octahedra should host the Mn(III) atoms.²⁰ Additionally, they determined the density to (3.86 ± 0.05) g/cm³, performed magnetic measurements between 4.2 and 300 K and determined the Néel temperature of the compound to $T_N = 54 \pm 3$ K, the

Weiss temperature to $\theta_p = -45 \pm 5$ °C, and the Curie constant to $C_M = 7.29 \pm 5$ cm³ K/mol.²⁰ The formation of Mn₂F₅ was confirmed as an intermediate phase during the decomposition process of MnF₃ to MnF₂.^{23,24}

We synthesized the compounds Mn₂F₅ and the so far unknown Mn₃F₈ by a high pressure/high-temperature method, determined their single crystal X-ray structures and used MAPLE and CHARDI calculations to verify the oxidation states. The compounds were additionally characterized by IR and Raman spectroscopy and magnetic measurements. Quantum chemical calculations reproduced the experimentally determined structures, support the assignment of the oxidation states, and allowed for the band assignments of the IR and Raman spectra.

Results and Discussion

Mn₂F₅ and Mn₃F₈ were obtained by compressing respective stoichiometric mixtures of MnF₂ and MnF₃ inside platinum capsules using a multi-anvil press (for details see the Experimental Section). A photo of the pink powder of Mn₂F₅, with some pale pink MnF₂ as impurity, is shown in Figure 1 and a photo of the violet powder of Mn₃F₈ is shown in Figure 3. We also obtained Mn₂F₅ by heating a stoichiometric mixture of MnF₂ and MnF₃ inside a sealed platinum ampoule up to 300 °C.

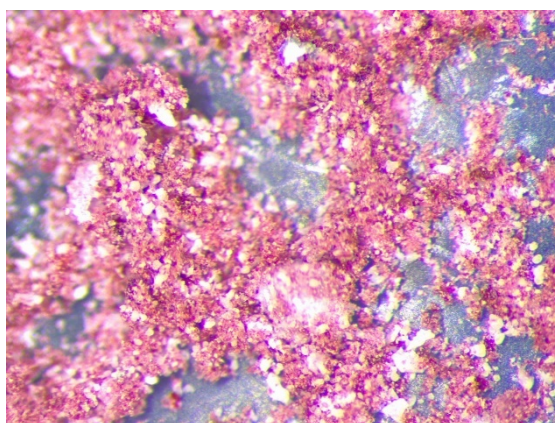


Figure 1. Photo of a sample of Mn₂F₅ containing significant amounts of pale pink MnF₂ as a secondary phase under an optical microscope.

The bulk composition of the Mn₂F₅ obtained from the multi-anvil press was analyzed by powder X-ray diffraction, the pattern and the Rietveld refinement are shown in Figure 2, details of the latter are available from Table 1 and Table S3. The lattice parameters are $a =$

8.686(3), $b = 6.153(3)$, $c = 7.775(3)$ Å, $\beta = 117.39(3)^\circ$, $V = 368.9(3)$ Å³, at $T = 293$ K. Despite the different measurement temperatures, these values are within tripled standard uncertainty or relatively close to the lattice parameters determined by single crystal X-ray diffraction at $T = 173$ K, see below, indicating that temperature changes seem to have only small effects on them. Besides Mn₂F₅, two polymorphic crystalline phases of MnF₂ are present, the tetragonal modification ($P4_2/mnm$) with circa 7(1) % and the orthorhombic one ($Pbcn$) with circa 58(2) %. So, the phase purity of Mn₂F₅ is only circa 35(2) %. Atom positions and isotropic displacement parameters had to be fixed in the Rietveld refinement.

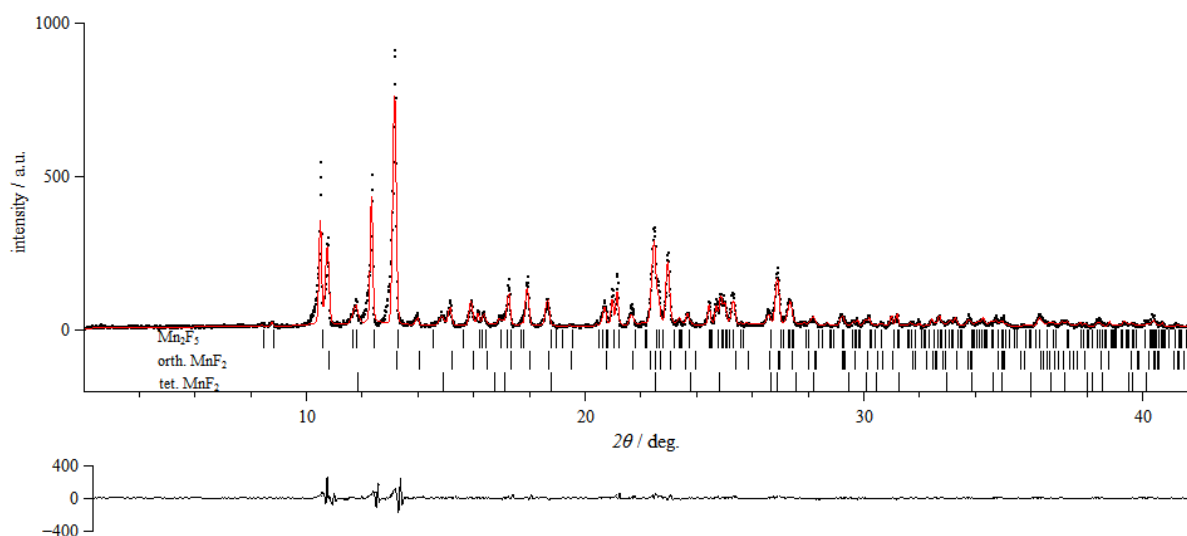


Figure 2. Rietveld refinement of the observed (black) and calculated (red) powder X-ray diffraction pattern of Mn₂F₅ (purity 35(2) %). The calculated reflection positions are indicated by the vertical bars below the pattern (first row Mn₂F₅, second and third row two different modifications of MnF₂). The curve at the bottom represents the difference between the observed and the calculated intensities. $R_p = 21.51$, $R_{wp} = 28.05$ (not background corrected R values), $S = 1.65$.

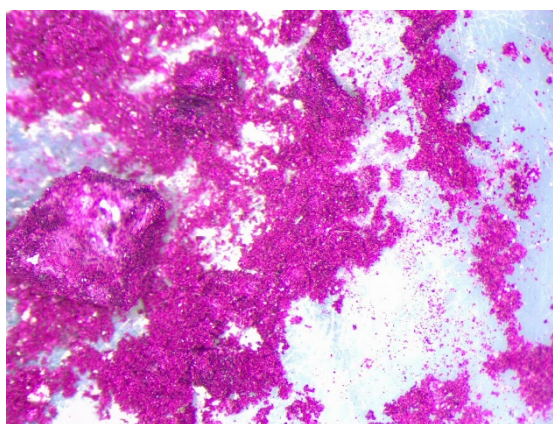


Figure 3. Photo of a sample of Mn₃F₈ containing small amounts of pale pink MnF₂ as a side phase under an optical microscope.

According to the powder X-ray diffraction pattern shown in Figure 4, Mn_3F_8 could also not be synthesized phase pure. There were always small amounts of MnF_2 present, likely in both modifications as well. The lattice parameters of Mn_3F_8 obtained by a Le-Bail fit are $a = 5.5329(6)$, $b = 4.8909(6)$, $c = 9.918(1)$ Å, $\beta = 92.616(7)^\circ$, $V = 268.12(6)$ Å³ at $T = 293$ K (Table 1).

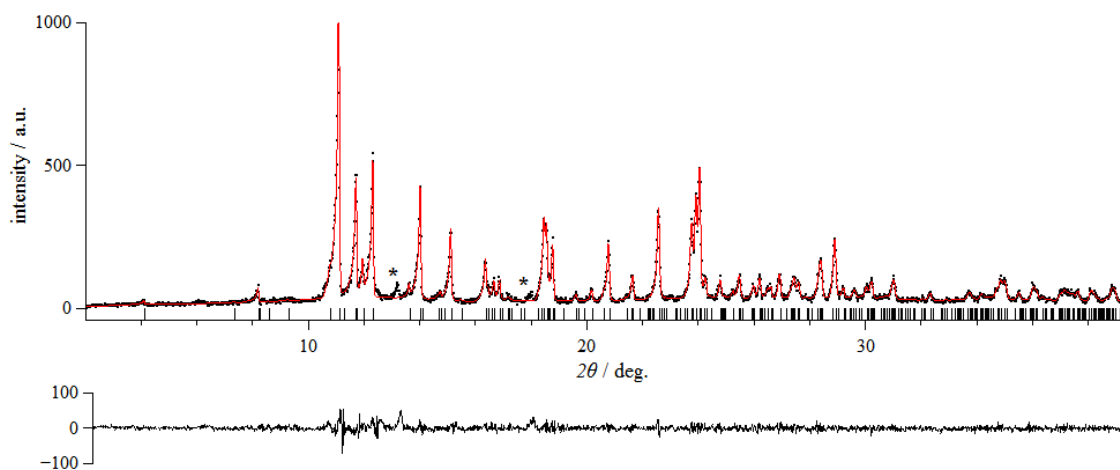


Figure 4. Le-Bail fit (red) on the observed (black) powder X-ray diffraction pattern of Mn_3F_8 . The calculated reflection positions are indicated by the vertical bars below the pattern and the curve at the bottom represents the difference between the observed and the calculated intensities. Asterisks denote reflections that belong to MnF_2 .

The crystal structure of Mn_2F_5

When *Hoppe* and coworkers first determined the crystal structures of CaMnF_5 and CdMnF_5 , twinning of the crystals led to problems. They originally concluded that CaMnF_5 and CdMnF_5 would crystallize in different space groups $P2/c$ and $P12_1/n1$, respectively.^{25,26} For CaMnF_5 they reported that both types of Jahn-Teller distortions, elongation and compression, are present for the $[\text{MnF}_6]^{3-}$ anions. Müller later revised these statements and showed that both compounds crystallize in the CaCrF_5 (MnCrF_5) structure type with space group $C2/c$.^{27,28} He showed that twinning was responsible for the observed violations of the extinction conditions for C -centering as well as for the false observation of elongated and compressed $[\text{MnF}_6]^{3-}$ octahedra within CaMnF_5 .²⁸ In the correct space group the Mn–F distances became equivalent and no unusual Jahn-Teller distortions were observable.²⁸ An example for the presence of both types of Jahn-Teller distortion within a compound is K_3MnF_6 .²⁹

All of the crystals of Mn_2F_5 selected by us for the diffraction experiment turned out to be twins. The compound Mn_2F_5 , that is Mn(II)Mn(III)F_5 , also crystallizes isotypic to CaCrF_5 (MnCrF_5) in the monoclinic crystal system in space group $C2/c$ (no. 15). The lattice

parameters determined by single crystal X-ray diffraction are $a = 8.7078(8)$, $b = 6.1473(6)$, $c = 7.7817(7)$ Å, $\beta = 117.41(1)^\circ$, $V = 369.80(6)$ Å³, with $Z = 4$, $mC28$, $15f^2e^2a$, at $T = 173$ K. Selected crystallographic data and details of the structure determination are available from Table 1.

Table 1. Selected crystallographic data and details of the structure determination of Mn₂F₅ and Mn₃F₈.

	single crystal	powder	single crystal	powder
Empirical formula	Mn ₂ F ₅		Mn ₃ F ₈	
Molar mass / g mol ⁻¹	204.88		316.84	
Crystal system	Monoclinic		Monoclinic	
Space group	<i>C2/c</i> (no. 15)		<i>P2₁</i> (no. 4)	
Single-crystal diffractometer	Bruker D8 Quest Photon 100	Stoe Stadi P	Bruker D8 Quest Photon 100	Stoe Stadi P
Radiation	Mo- <i>K</i> _α ($\lambda = 0.7107$ Å)	Mo- <i>K</i> _{α1} ($\lambda = 0.7093$ Å)	Mo- <i>K</i> _α ($\lambda = 0.7107$ Å)	Mo- <i>K</i> _{α1} ($\lambda = 0.7093$ Å)
<i>a</i> / Å	8.7078(8)	8.686(3)	5.5253(2)	5.5329(6)
<i>b</i> / Å	6.1473(6)	6.153(3)	4.8786(2)	4.8909(6)
<i>c</i> / Å	7.7817(7)	7.775(3)	9.9124(4)	9.918(1)
β / °	117.41(1)	117.39(3)	92.608(2)	92.616(7)
<i>V</i> / Å ³	369.80(6)	368.9(3)	266.92(2)	268.12(6)
Formula units per cell (<i>Z</i>)	4		2	
Calculated density / g cm ⁻³	3.680	3.6884	3.942	
Temperature / K	173.0	293	183.0	293
Absorption coefficient / mm ⁻¹	6.812	6.547	7.097	
<i>F</i> (000)	380		294	
Crystal size / mm ³	0.03 × 0.03 × 0.02	powder	0.03 × 0.03 × 0.02	powder
2 θ range / °	8.5 – 79.2	2.000 – 41.885	4.1 – 80.5	
Collected reflections	941		12839	
Independent reflections / ref. parameters / <i>R</i> _{int}	941 / 37 / 0.0478		3336 / 101 / 0.0362	
Goodness-of-fit on <i>F</i> ²	1.085	1.65	1.107	
Final <i>R</i> indices [$I \geq 2\sigma$ (<i>I</i>)]	$R_1 = 0.0269$, $wR_2 = 0.0488$		$R_1 = 0.0288$, $wR_2 = 0.0547$	
Final <i>R</i> indices [all data]	$R_1 = 0.0375$, $wR_2 = 0.0520$		$R_1 = 0.0442$, $wR_2 = 0.0670$	
Largest diff. peak/hole / e Å ⁻³	0.72 / -0.64		0.68 / -1.20	
Twin fraction	0.209(4)		0.42(3)	

Atomic coordinates and isotropic displacement parameters are given in Table 2, anisotropic ones in the Supporting Information (Table S1). The atom names and positions were chosen in analogy to CaCrF_5 .²⁷

Table 2. Wyckoff positions, site symmetries, atomic coordinates and equivalent isotropic displacement parameters U_{iso} for Mn_2F_5 .

Atom	Position, Symmetry	x	y	z	$U_{\text{iso}} / \text{\AA}^2$
Mn(1)	$4a, \bar{1}$	0	0	0	0.00462(9)
Mn(2)	$4e, 2$	0	0.46580(5)	$\frac{1}{4}$	0.00698(9)
F(1)	$4e, 2$	0	0.1214(2)	$\frac{1}{4}$	0.0105(3)
F(2)	$8f, 1$	0.48129(15)	0.20396(15)	0.04486(16)	0.0131(2)
F(3)	$8f, 1$	0.23501(12)	0.02702(17)	0.6283(2)	0.0148(2)

Two crystallographically independent Mn atoms, Mn(1) and Mn(2), reside on Wyckoff sites $4a$ and $4e$, respectively, while three symmetry-independent F atoms are located at the Wyckoff positions $4e$ (F(1)) and $2 \times 8f$ (F(2) and F(3)). The Mn(1) atom, residing on an inversion center, is coordinated octahedron-like by six F atoms ($2 \times \text{F}(1)$, $2 \times \text{F}(2)$, $2 \times \text{F}(3)$), see Figure 5.

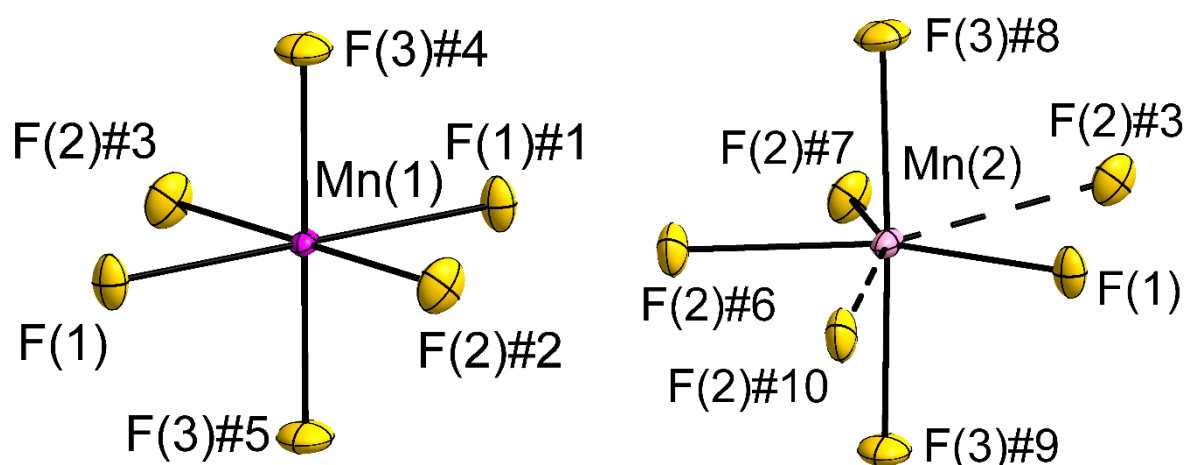


Figure 5. Sections of the crystal structure of Mn_2F_5 . Left: Octahedron-like coordination sphere around the Mn^{III} (1) atom. Right: Trigonal bipyramidal-like coordination sphere around the Mn^{II} atom Mn(2). F atoms in yellow, the Mn(III) atom Mn(1) in pink, the Mn(II) atom Mn(2) in rose color. The dashed bonds indicate the long contacts with circa 2.6 Å. Displacement ellipsoids are shown at the 70% probability level at 173 K. Symmetry transformations for the generation of equivalent atoms: #1 $-x, -y, -z$, #2 $-\frac{1}{2} + x, -\frac{1}{2} + y, z$, #3 $\frac{1}{2} - x, \frac{1}{2} - y, -z$, #4 $x, -y, -\frac{1}{2} + z$, #5 $-x, y, \frac{1}{2} - z$, #6 $\frac{1}{2} - x, \frac{1}{2} + y, \frac{1}{2} - z$, #7 $-\frac{1}{2} + x, \frac{1}{2} + y, z$, #8 $\frac{1}{2} - x, \frac{1}{2} - y, 1 - z$, #9 $-\frac{1}{2} + x, \frac{1}{2} - y, -\frac{1}{2} + z$, #10 $-\frac{1}{2} + x, \frac{1}{2} - y, \frac{1}{2} + z$.

The Mn(1)–F bond lengths are 2.0836(5) Å for F(1), 1.8742(9) Å for F(2), and 1.8252(10) Å for F(3), see Table 3. These bond lengths are typical for elongated $[\text{MnF}_6]^{3-}$ octahedra in $\text{K}_3[\text{MnF}_6]^{29}$ or $\text{Na}_3[\text{MnF}_6]^{30}$ and therefore we assign the Mn(1) atom the oxidation state +III. This assignment is in line with the observed Mn(2)–F bond lengths (Table 3), that are longer with 2.1173(13) Å for F(1), 2.1163(10) Å for F(2), and 2.0522(10) Å for F(3), despite a smaller coordination number for Mn(2) of five. Therefore we assign oxidation state +II to the Mn(2) atom. The assignment of oxidation states is also in line with compounds crystallizing in the same structure type, with $M(\text{III})$ on the $4a$ and $M(\text{II})$ on the $4e$ Wyckoff positions.

Table 3. Selected interatomic distances d and their multiplicities m for Mn_2F_5 .

Atom 1	Atom 2	m	$d / \text{Å}$
Mn ^{III} (1)	F(1)	2	2.0836(5)
	F(2)	2	1.8742(9)
	F(3)	2	1.8252(10)
Mn ^{II} (2)	F(1)	1	2.1173(13)
	F(2)	2	2.1163(10)
	F(3)	2	2.0522(10)

The coordination sphere of the Mn(2) atom can be described as trigonal bipyramidal, however, the two equatorial F(1)–Mn(2)–F(2) angles are widened to circa 134° while the third equatorial F(2)–Mn(2)–F(2) angle is narrowed to approximately only 92°. The widening is due to two additional Mn(2)⋯F(2) contacts, shown dashed in Figure 5, within the virtual equatorial plane that are with a distance of 2.5931(12) Å considerably longer than the Mn(2)–F bonds. If these are considered, then distorted pentagonal bipyramids result as the coordination polyhedra for the Mn(2) atoms.

With these simple coordination spheres as a model, the fluoride anions F(2) and F(3) are μ_2 -like bridging between Mn(1) and Mn(2) atoms, while the F(1) atoms are μ_3 -like bridging between two Mn(1) and one Mn(2) atoms. Via these interconnections a three-dimensional infinite network structure is formed for MnMnF_5 which can be described by the Niggli formula $\infty^3[\langle \text{Mn}(\text{II})\text{F}_{\frac{1}{1+2}}\text{F}_{\frac{4}{1+1}} \rangle \langle \text{Mn}(\text{III})\text{F}_{\frac{2}{2+1}}\text{F}_{\frac{4}{1+1}} \rangle]$ with the notation of the formula according to the literature.³¹ Explained in short, this type of Niggli formula indicates for the Mn(II) cation that one F atom bridges μ_3 -like between a Mn(II) and two Mn(III) atoms, and four F atoms bridge between the Mn(II) and a Mn(III) atom. For the Mn(III) atom, there are two μ_3 -like bridging F atoms between two Mn(III) and one Mn(II) atom, and four μ_2 -like bridging F

atoms between the Mn(III) and a Mn(II) atom. The octahedron-like $[\text{Mn(III)F}_6]^{3-}$ anions form one-dimensional infinite strands of trans-corner-connected octahedra that run parallel to the c axis with the Mn(II) ions residing in between and connecting them (Figure 6).

Topologically, the crystal structure is related to the NaCl structure type. The Mn(1) atoms are cubic close packed with Mn(2) atoms in all octahedral voids and vice versa (Figure 6). The F atoms reside in between at no special positions regarding this packing and are μ_2 - as well as μ_3 -like bridging between the Mn atoms as described above. The crystal structure of Mn_2F_5 is shown in Figure 6.

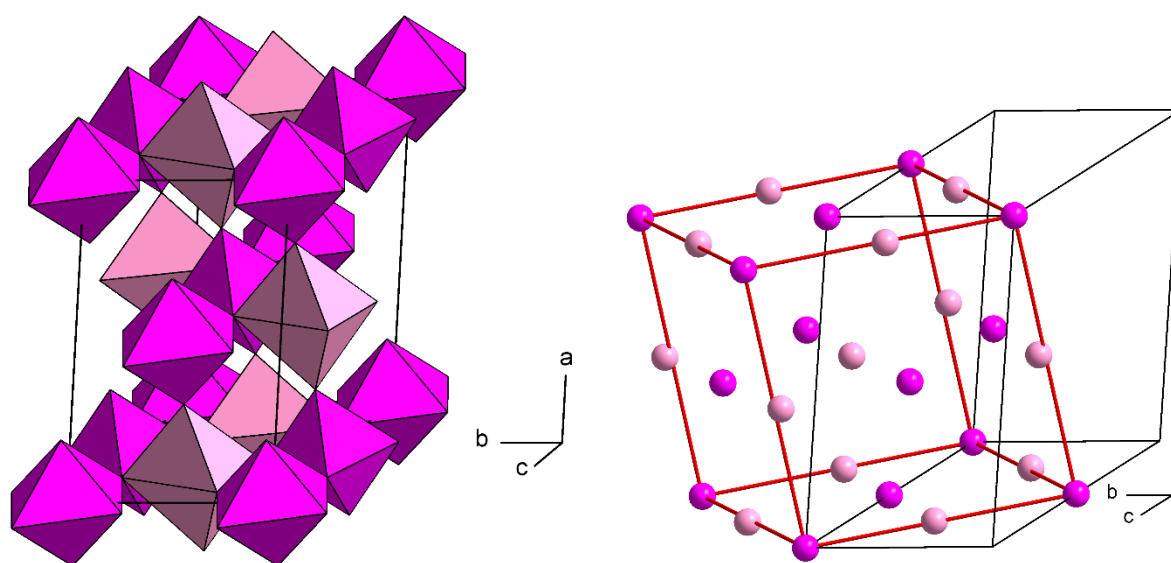


Figure 6. The crystal structure of Mn_2F_5 is depicted on the left. The coordination polyhedra show the surrounding of the Mn atoms by F atoms. Trigonal-bipyramidal coordination polyhedra of Mn(II) atoms in rose color, coordination octahedra of Mn(III) atoms in pink color. On the right the relation of the crystal structure of Mn_2F_5 to the NaCl structure type is displayed. The black unit cell is the monoclinic one, while the red represents the pseudo-cubic unit cell Mn(II) atoms in rose, Mn(III) atoms in pink.

Tressaud and *Dance* had reported the lattice parameters of Mn_2F_5 in 1974 as $a = (15.44 \pm 0.02)$, $b = (7.27 \pm 0.01)$, $c = (6.17 \pm 0.01)$ Å, $V \approx 693$ Å³,²⁰ as they suspected that the structure should be related to MnCrF_5 , which had been reported orthorhombic, space group $Cmmm$ with $a = (15.486 \pm 0.003)$, $b = (7.381 \pm 0.003)$, $c = (6.291 \pm 0.003)$ Å, $V \approx 719$ Å³ in 1971.²¹ Later, MnCrF_5 was corrected to be monoclinic, space group $C2/c$ with the lattice parameters $a = 8.856(5)$, $b = 6.291(3)$, $c = 7.381(4)$ Å, $\beta = 115.46(7)^\circ$, $V \approx 371$ Å³.²² The monoclinic and the orthorhombic unit cells are related by equation 1.

$$\begin{pmatrix} \mathbf{a}_{orth} \\ \mathbf{b}_{orth} \\ \mathbf{c}_{orth} \end{pmatrix} = \begin{pmatrix} 2 & 0 & 1 \\ 0 & 0 & -1 \\ 0 & 1 & 0 \end{pmatrix} \begin{pmatrix} \mathbf{a}_{mon} \\ \mathbf{b}_{mon} \\ \mathbf{c}_{mon} \end{pmatrix} \quad (1)$$

Our lattice parameters for Mn_2F_5 are $a_{\text{mon}} = 8.7078(8)$, $b_{\text{mon}} = 6.1473(6)$, $c_{\text{mon}} = 7.7817(7)$ Å, $\beta_{\text{mon}} = 117.41(1)^\circ$, $V = 369.80(6)$ Å³ which leads to $a_{\text{orth}} = 15.462$, $b_{\text{orth}} = 7.782$, $c_{\text{orth}} = 6.147$ Å, $\gamma_{\text{orth}} = 89.1^\circ$, $V = 739$ Å³. It is obvious how close these values are to the ones determined by *Tressaud and Dance*.

Crystal Structure of Mn_3F_8

Mn_3F_8 crystallizes in the monoclinic crystal system in the space group $P2_1$ (no. 4) with the lattice parameters $a = 5.5253(2)$, $b = 4.8786(2)$, $c = 9.9124(4)$ Å, with $\beta = 92.608(2)^\circ$, $V = 266.92(2)$ Å³, $Z = 2$, $mP22$, $4a^{11}$, at $T = 183$ K. Selected crystallographic data and details of the structure determination are available from Table 1. Atomic coordinates and isotropic displacement parameters are given in Table 4, anisotropic ones in the Supporting Information (Table S2). To the best of our knowledge, Mn_3F_8 represents a novel structure type.

Table 4. Wyckoff positions, site symmetries, atomic coordinates and equivalent isotropic displacement parameters U_{iso} for Mn_3F_8 .

Atom	Position, Symmetry	x	y	z	$U_{\text{iso}} / \text{Å}^2$
Mn ^{III} (1)	$2a, 1$	0.24833(8)	0	-0.00454(4)	0.00423(7)
Mn ^{II} (2)	$2a, 1$	0.39842(7)	0.0095(2)	0.34388(4)	0.00625(9)
Mn ^{III} (3)	$2a, 1$	0.10590(7)	-0.0021(2)	-0.36141(4)	0.00440(8)
F(1)	$2a, 1$	0.0494(3)	0.2772(6)	-0.06113(19)	0.0082(4)
F(2)	$2a, 1$	0.4466(3)	-0.2748(6)	0.05865(19)	0.0084(4)
F(3)	$2a, 1$	0.2775(4)	0.1616(6)	0.16602(18)	0.0093(4)
F(4)	$2a, 1$	0.2213(3)	-0.1547(6)	-0.17899(18)	0.0078(3)
F(5)	$2a, 1$	-0.0748(3)	-0.3054(5)	-0.42719(18)	0.0073(3)
F(6)	$2a, 1$	0.3860(3)	-0.1547(5)	-0.43713(18)	0.0074(3)
F(7)	$2a, 1$	-0.1773(3)	0.1607(6)	-0.32269(18)	0.0088(4)
F(8)	$2a, 1$	0.2805(4)	0.3117(6)	-0.3271(2)	0.0087(3)

All atoms are located on Wyckoff site $2a$ and the three crystallographically independent Mn atoms are surrounded by six F atoms, each (Figure 7). The crystal structure is not centrosymmetric. While the Mn(1) atom resides on a pseudo inversion center and its coordination sphere is close to being inversion symmetric (see below and Figure 7), the coordination spheres of the neighboring Mn(2) and Mn(3) atoms are much too different: The coordination polyhedron around the Mn(1) atom is closest to an octahedron with F–Mn–F_{cis} bond angles of $88.46(9)^\circ$ to $92.68(10)^\circ$ and F–Mn–F_{trans} angles within $176.72(8)$ to

178.50(14)°. The coordination octahedron around Mn(2) is most distorted with the respective angles from 76.81(8) to 111.23(8)° and from 158.61(7) to 162.50(8)°, only. Finally, the one around Mn(3) shows respective angles of 80.35(7) to 102.20(8)° and 165.86(7) to 170.36(9)°.

The oxidation states of the Mn atoms can be inferred from their respective distances to the F atoms. For the Mn(1) atom the six Mn–F bonds are approximately 2×1.82 , 1.87, 1.89, and 2×2.10 Å long and agree with those observed for neat MnF₃ and for the [MnF₆]³⁻ anions in Na₃[MnF₆].^{10,30} Selected bond lengths are available from Table 5. For the Mn(3) atom, they are in a similar range compared to those of the Mn(1) atom with circa 1.81, 1.83, 1.89, 1.90, 2.03 Å, however, one longer Mn–F bond of 2.304(2) Å is present (shown dashed in Figure 7). In contrast to the bond lengths of the Mn(1) and Mn(3) atoms, all Mn(2)–F bond lengths are above 2 Å with circa 2.0, 2.03, 2.10, 2×2.20 Å, and also one longer Mn–F bond with 2.3177(19) Å is present (also shown dashed in Figure 7). We therefore assign oxidation state +II to the latter Mn(2) atom, while the Mn(1) and Mn(3) atoms have oxidation state +III, each.

Table 5. Selected bond lengths for Mn₃F₈. Bond lengths ordered ascending within the columns. Symmetry transformations for the generation of equivalent atoms: #1 $-x, -\frac{1}{2} + y, -z$; #2 $1 - x, \frac{1}{2} + y, -z$; #3 $-x, \frac{1}{2} + y, -1 - z$; #4 $-x, \frac{1}{2} + y, -z$; #5 $x, y, 1 + z$; #6 $1 - x, -\frac{1}{2} + y, -z$.

Atom 1	Atom 2	<i>d</i> / Å	Atom 1	Atom 2	<i>d</i> / Å	Atom 1	Atom 2	<i>d</i> / Å
Mn ^{III} (1)	F(1)	1.816(2)	Mn ^{II} (2)	F(3)	2.000(2)	Mn ^{III} (3)	F(7)	1.8111(19)
	F(2)	1.824(2)		F(8)#6	2.033(2)		F(8)	1.833(2)
	F(3)	1.866(2)		F(5)#4	2.197(2)		F(5)	1.885(2)
	F(4)	1.8863(19)		F(6)#2	2.204(2)		F(6)	1.9025(19)
	F(1)#1	2.100(2)		F(7)#1	2.100(2)		F(4)	2.031(2)
	F(2)#2	2.102(2)		F(6)#5	2.3177(19)		F(5)#3	2.304(2)

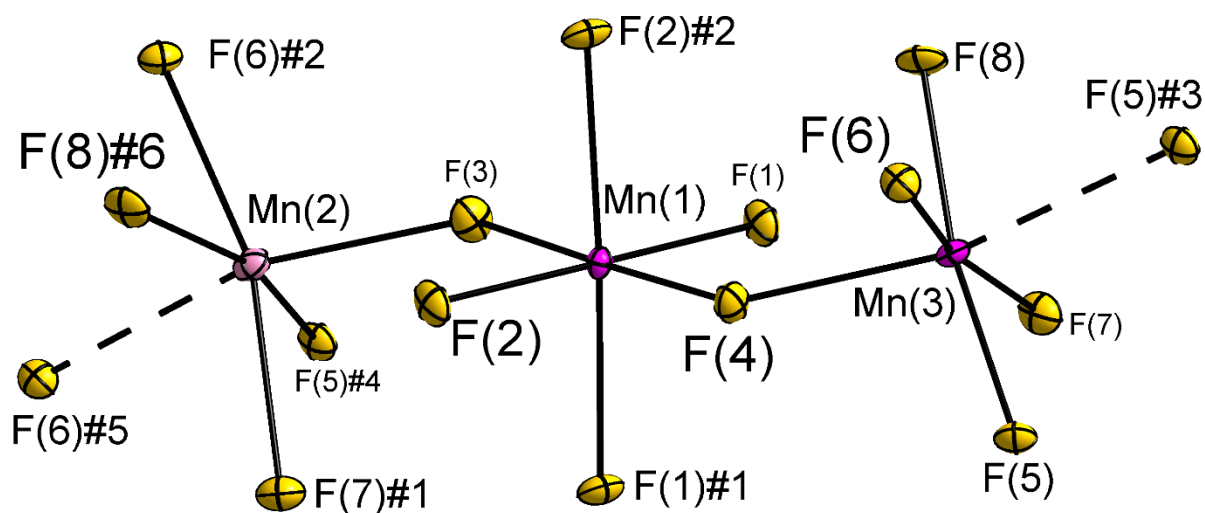


Figure 7. A section of the crystal structure of Mn_3F_8 showing the coordination spheres of the Mn atoms. Mn(II) atom in rose color, Mn(III) atoms in pink color. The pseudo inversion center on the Mn(1) atom is evident. The Mn–F bonds longer than 2.3 Å are shown dashed. Displacement ellipsoids are shown at the 70% probability level at 183 K. Symmetry transformations for the generation of equivalent atoms: #1 $-x, -\frac{1}{2} + y, -z$; #2 $1 - x, \frac{1}{2} + y, -z$; #3 $-x, \frac{1}{2} + y, -1 - z$; #4 $-x, \frac{1}{2} + y, -z$; #5 $x, y, 1 + z$; #6 $1 - x, -\frac{1}{2} + y, -z$.

The F(1) and F(2) atoms bridge μ -like to other Mn(1) atoms exclusively, while the F(3) atom connects to a Mn^{II}(2) atom and the F(4) atom to a Mn^{III}(3) atom (Figure 7). The other fluorine atoms F(5) to F(8) interconnect exclusively the Mn^{II}(2) and the Mn^{III}(3) atoms, with F(5) and F(6) bridging μ_3 -like, and F(7) and F(8) μ -like. So, the coordination octahedra of Mn^{III}(1) are exclusively corner-sharing, while the coordination polyhedra of Mn^{II}(2) and Mn^{III}(3) share common corners as well as edges (Figure 8). The Mn^{III}(1) coordination polyhedra form imaginary (mono)layers of corner-connected octahedra (white edges in Figure 8) parallel to the *ab* plane. The Mn^{II}(2) and Mn^{III}(3) coordination polyhedra form corner and edge connections (black edges in Figure 8) and reside in between the Mn(I) layers. The crystal structure is best described as an imaginary triple layer, in which the (mono)layer of Mn(1) coordination octahedra is sandwiched between a layer of alternating Mn(2) and Mn(3) coordination polyhedra. These triple layers are interconnected along the *c* axis by the 2.3 Å long Mn–F bonds shown dashed in Figure 8. Overall, a three-dimensional infinite network structure results that can be described with the Niggli formula

$$\left[\langle \text{Mn}^{\text{II}}(2) \text{F}_{\frac{1}{1+1+0}} \text{F}_{\frac{2}{0+1+1}} \text{F}_{\frac{2}{0+2+1}} \text{F}_{\frac{1}{0+1+2}} \rangle \langle \text{Mn}^{\text{III}}(1) \text{F}_{\frac{4}{0+2+0}} \text{F}_{\frac{1}{1+1}} \text{F}_{\frac{1}{0+1+1}} \rangle \langle \text{Mn}^{\text{III}}(3) \text{F}_{\frac{1}{0+1+1}} \text{F}_{\frac{2}{1+0+1}} \text{F}_{\frac{2}{0+1+2}} \text{F}_{\frac{1}{0+2+1}} \rangle \right]_{\infty}$$

which also illustrates the coordination spheres and the connectivity of the different Mn and F atoms.³¹ The first number in the denominator refers to Mn^{II}(2), the second to Mn^{III}(1), and the

third to Mn^{III}(3), as indicated by the Niggli formula. The crystal structure of Mn₃F₈ is shown in Figure 8.

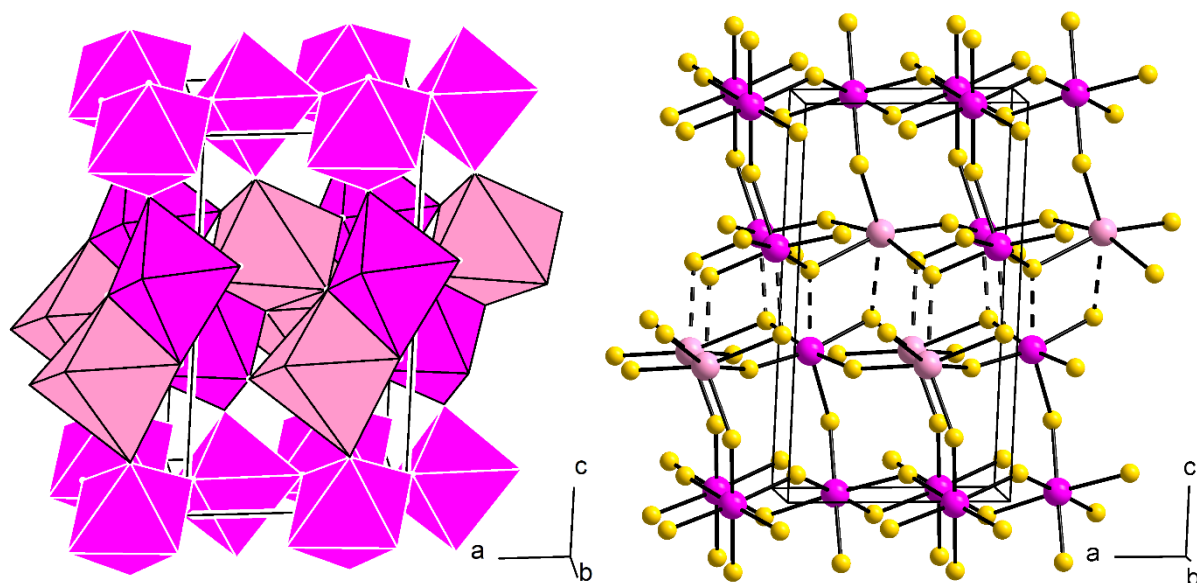


Figure 8. The crystal structure of Mn₃F₈. Left: Pink coordination polyhedra denote those of Mn(III), rose ones stand for those of Mn(II). The imaginary (mono)layer of Mn(1) coordination octahedra is indicated by white edges, the Mn(2) and Mn(3) coordination polyhedra are shown with black edges. Right: Dashed bonds indicate the long Mn–F bonds interconnecting the triple layers.

Topologically, the Mn(1) atoms form a slightly corrugated net of rhombuses in the *ab* plane. The centers of gravity between neighboring Mn(2) and Mn(3) atoms form a slightly more corrugated net of rhombuses at $z \approx \frac{1}{2}$ which is superimposed on the net at $z = 0$. To the best of our knowledge, Mn₃F₈ represents a novel structure type.

Calculations of BLBS, CHARDI and MAPLE values

To evaluate and further support the crystal structure refinements, bond valence sums (BVS) and MAPLE values (MAdelung Part of Lattice Energy) were calculated for Mn₂F₅ as well as for Mn₃F₈.^{32–34} Table 6 contains the charge distributions calculated via the bond length-bond strength (BLBS)^{35,36} and charge distribution (CHARDI)^{37,38} concepts. The BLBS concept uses the correlation of bond length and bond strength (bond valences) to predict the formal oxidation state of an atom. The sum of all bond valences should add up to the oxidation state of the respective atom. The CHARDI method on the other hand, combines the concept of effective coordination numbers (ECoNs) with Pauling's concept of bond strength to calculate the charge distribution in inorganic solids.

Table 6. Charge distribution in Mn₂F₅ and Mn₃F₈ calculated via BLBS (ΣV) and CHARDI (ΣQ).

Mn ₂ F ₅	Mn(1)	Mn(2)	F(1)	F(2)	F(3)						
ΣV	3.04	1.91	-0.96	-0.88	-1.02						
ΣQ	2.99	2.01	-0.85	-0.97	-1.10						
Mn ₃ F ₈	Mn(1)	Mn(2)	Mn(3)	F(1)	F(2)	F(3)	F(4)	F(5)	F(6)	F(7)	F(8)
ΣV	3.35	1.70	2.90	-0.96	-0.94	-0.97	-0.91	-1.00	-0.96	-1.00	-1.03
ΣQ	3.19	1.89	2.92	-0.92	-0.90	-1.09	-0.90	-0.92	-0.99	-1.12	-1.15

Bond valence sums calculated for Mn₂F₅ suggest a charge of +2 for the Mn^{II}(2) atom in distorted pentagonal bipyramidal coordination and a charge of +3 for the Mn(1) atom in octahedral coordination. These results are in accordance with the oxidation states reported for the isotypic compounds MnCrF₅³⁹ and CaCrF₅.⁴⁰ For Mn₃F₈, the calculations suggest a charge of +2 for the Mn(2) atom, while the Mn(1) and Mn(3) atoms are expected to have an oxidation state of +3. For both compounds our calculations agree with the assignment of oxidation states based on crystallographic criteria.

In Table 7, the calculated MAPLE values for Mn₂F₅ and Mn₃F₈ are compared to the calculated MAPLE values from the starting materials MnF₂ (rutile Type)⁴¹ and MnF₃.⁸

Table 7. Comparison of the MAPLE values calculated for Mn₂F₅ and Mn₃F₈ with the sums of MAPLE values calculated for MnF₂ (rutile type) and MnF₃.

	MAPLE of MnF ₂ ⁴¹ / kJ mol ⁻¹	MAPLE of MnF ₃ ⁸ / kJ mol ⁻¹	Respective sum of MnF ₂ /MnF ₃ MAPLE values / kJ mol ⁻¹	MAPLEs of title compounds / kJ mol ⁻¹	Difference of MAPLE values / %
Calc. for Mn ₂ F ₅ case	3149	6453	9602	9600	0.02
Calc. for Mn ₃ F ₈ case	3149	2 × 6453	16055	15936	0.74

The calculations show a discrepancy in the MAPLE values of only 0.02 % for Mn₂F₅ and 0.74 % for Mn₃F₈, further indicating plausible structure models.

Quantum chemical calculations

We investigated the structure and properties of Mn_2F_5 , Mn_3F_8 , and MnF_2 (rutile type) using quantum chemical methods (DFT-PBE0/TZVP level of theory, see Computational details). We ran the quantum chemical calculations for several different magnetic configurations. For the ferromagnetic configurations and the ferrimagnetic configuration of Mn_2F_5 , we applied the primitive cells as such. For the investigation of possible antiferromagnetic and ferrimagnetic orderings of Mn_2F_5 and Mn_3F_8 , the space group was changed to $P1$. The optimized geometries of the studied magnetic configurations are given in the Supporting information. Harmonic frequency calculations showed the optimized structures to be true local minima.

For MnF_2 , quantum chemical calculations were carried out for both the rutile type tetragonal polymorph ($P42/mnm$)⁴² and the orthorhombic polymorph ($Pbcn$)⁴³ accessible at high pressures, as both were experimentally observed. The antiferromagnetic configurations used in the quantum calculations have been previously determined by Golosovsky and coworkers.⁴⁴ Taking the magnetic configurations into account reduced the space group of the tetragonal structure to $Cmmm$ and that of the orthorhombic structure to $P2/c$. The tetragonal MnF_2 structure is 0.2 kJ/mol per Mn atom lower in energy compared to the orthorhombic polymorph, in agreement with the reported metastable nature of the latter.^{44,45} The electronic band gap is 6.2 eV for both polymorphs.

For Mn_2F_5 , the ferromagnetic ordering and the lowest-energy antiferromagnetic ordering have essentially the same energy. For Mn_3F_8 , the lowest-energy ferrimagnetic ordering is only 0.2 kJ/mol per Mn atom higher in energy compared to the ferromagnetic ordering, which is a negligible difference considering the used level of theory. The presented antiferromagnetic and ferrimagnetic orderings are also in line with magnetic measurements presented below. MnCrF_5 , with which Mn_2F_5 is isotypic, has previously been reported to have an antiferromagnetic ordering.²² A full energy comparison for the studied magnetic configurations is included as Supporting Information.

The geometries of the optimized structures are in good agreement with the experimentally determined crystal structures. For antiferromagnetic Mn_2F_5 , the differences in the lattice parameters a , b , and c are small with $\Delta a = 1.0\%$, $\Delta b = 1.1\%$, and $\Delta c = 1.2\%$, indicating a good agreement. The $\text{Mn}^{\text{II}}(2)\text{-F}$ distances of 2.07 Å (2×), 2.12 Å (2×), and 2.14 Å and $\text{Mn}^{\text{III}}(1)\text{-F}$ distances of 1.84 Å (2×), 1.88 Å, 1.89 Å, 2.11 Å, and 2.12 Å also agree with the experiment. For ferrimagnetic Mn_3F_8 , the differences in lattice parameters are $\Delta a = 2.6\%$, Δb

= 1.1%, $\Delta c = 2.7\%$. In Mn_3F_8 , the $\text{Mn}^{\text{II}}(2)\text{-F}$ distances are over 2.0 Å (2.00 Å, 2.06 Å, 2.12 Å, 2.20 Å, 2.23 Å, and 2.37 Å). The $\text{Mn}^{\text{III}}(1)\text{-F}$ distances are 1.82 Å, 1.83 Å, 1.89 Å, 1.91 Å, and 2.12 Å (2×) and the $\text{Mn}^{\text{III}}(3)\text{-F}$ distances are 1.82 Å, 1.84 Å, 1.90 Å, 1.91 Å, 2.03 Å, and 2.39 Å. The longest Mn–F distances of 2.37 Å and 2.39 Å are somewhat overestimated in comparison to the experiment, but otherwise the agreement with experiment is as good as for Mn_2F_5 .

Band gaps of antiferromagnetic Mn_2F_5 and ferrimagnetic Mn_3F_8 are 3.6 eV and 3.5 eV, respectively. The atomic spin populations, interpretable as the number of unpaired electrons, are in line with the derived oxidation states. In Mn_2F_5 , the spin populations are 3.9 for $\text{Mn}^{\text{III}}(1)$ and 4.9 for $\text{Mn}^{\text{II}}(2)$, close to the ideal values of 4 and 5, respectively (there are two Mn atoms per each position in the magnetically ordered model, but their spin populations are close to the average values listed here). In Mn_3F_8 , the spin populations are 3.9 for $\text{Mn}^{\text{III}}(1)$, 4.9 for $\text{Mn}^{\text{II}}(2)$, and 3.9 for $\text{Mn}^{\text{III}}(3)$.

The computational results related to the interpretation of the IR and Raman spectra are discussed in detail below.

UV/Vis-Spectroscopy

UV/Vis spectra were collected of both Mn_2F_5 and Mn_3F_8 using a reflection method. The spectra are shown in Figure 9 and Figure 10 and the broad bands above 600 nm show the violet/pink colors of the compounds. For comparison, the UV/Vis spectrum of MnF_2 is available in Figure S9.

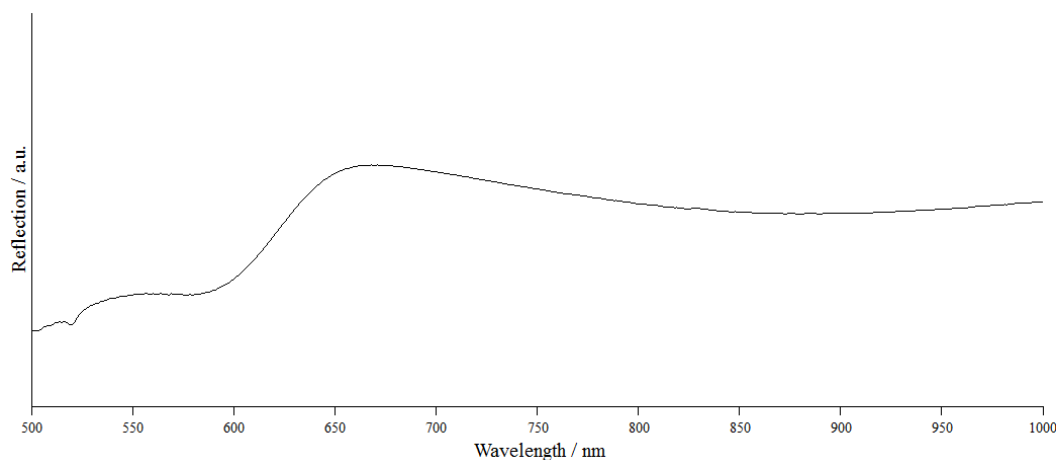


Figure 9. UV/Vis reflection spectrum of Mn_2F_5 .

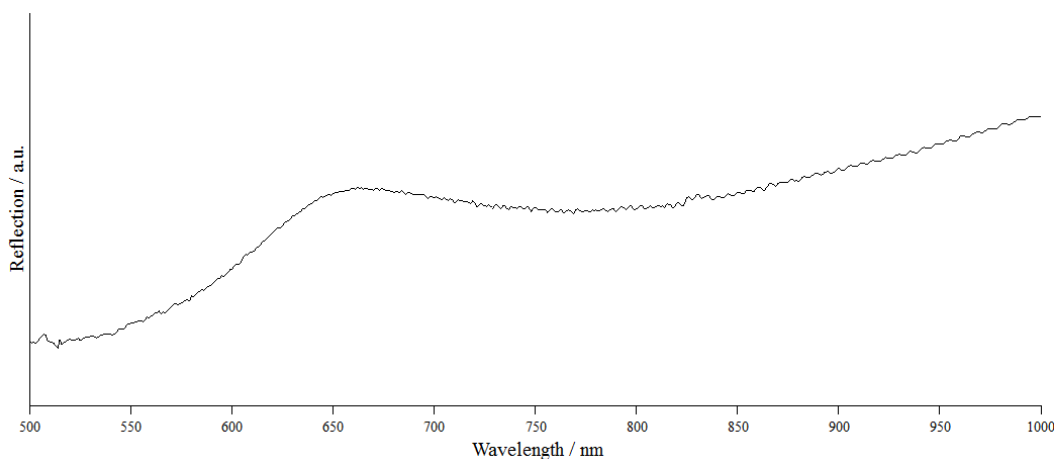


Figure 10. UV/Vis reflection spectrum of Mn_3F_8 .

Vibrational Spectroscopy on Mn_2F_5

Figure 11 and Figure 12 show sections of the vibrational spectra of Mn_2F_5 . The spectra were recorded on a sample which contained some MnF_2 as impurity. Complete spectra are given in the Supporting Information (Figures S1 and S2). For band assignments, which are given in Table 8, we also calculated the IR and Raman spectra with the DFT-PBE0 method. As discussed above, the calculations of antiferromagnetic Mn_2F_5 were carried out in space group $P1$. Compared with the experimentally determined spectra, the bands calculated within the harmonic approximation are shifted to smaller frequencies.

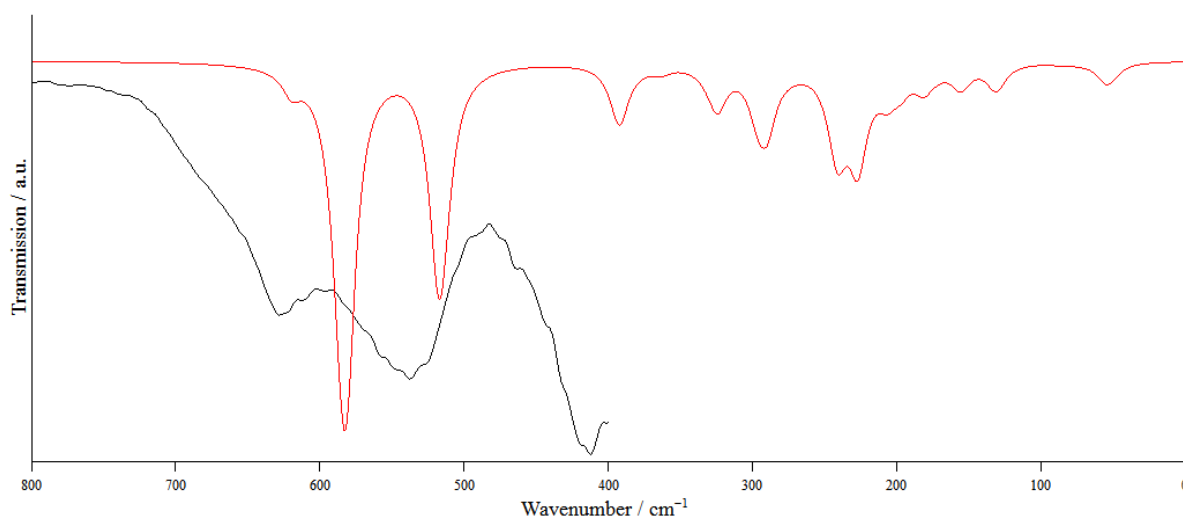


Figure 11. A section of the IR spectrum of Mn_2F_5 in black and the calculated DFT-PBE0 IR spectrum in red. The complete spectrum is given in the Supporting Information.

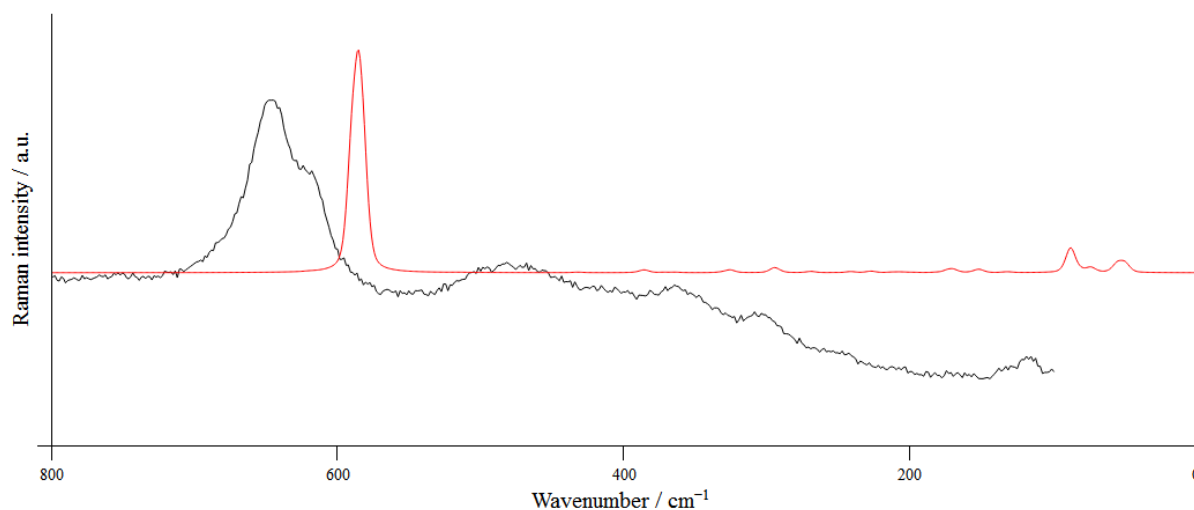


Figure 12. A section of the Raman spectrum of Mn_2F_5 in black and the calculated DFT-PBE0 spectrum in red. The complete spectrum is given in the Supporting Information.

Table 8. Assignment of the observed vibrations (obs., in cm^{-1}) of Mn_2F_5 , which contained some MnF_2 as impurity.

IR modes				
Observed	Calc. for Mn_2F_5	Assignment	Calc. for MnF_2 (tetragonal)	Calc. for MnF_2 (orthorhombic)
629	619	Mn–F(3) stretching		
	585, 581	Mn–F(3) stretching		
540	517, 512	Mn–F(2) stretching		
415	392	Mn–F(1) stretching		
	324, 296	Mn(2)–F(1) stretching, with Mn(1)–F bending	355	360, 322, 314
	290	Mn(1)–F(1) stretching, with Mn(1)–F bending	283	300, 293
	241, 227, 226	Mn–F(2) and Mn–F(1) bending		232,
	Below 200	Lattice vibrations	164	180, 133
Raman modes				
648				
622	589	Fully symmetric Mn(1)–F stretching		
	585, 581	Mn–F(3) stretching		
482 (broad)			473	469, 413
364	385	Mn(2)–F stretching		386, 384
	326	Mn(2)–F(1) stretching, with Mn(1)–F bending	335	
307	294	Mn–F(3) and Mn–F(2) bending		290
	269	Mn–F(3) and Mn–F(2) bending		264, 524
	241, 227, 226	Mn–F(2) and Mn–F(1) bending		229
117	Below 200	Lattice vibrations		

We also calculated the IR and Raman bands for MnF_2 (tetragonal and orthorhombic), to verify which bands arise from that impurity. According to this calculation, no IR bands should be observed in the region above 400 cm^{-1} for MnF_2 . However, both MnF_2 modifications should

be observable in the Raman spectrum with MnF_2 (tetragonal) bands calculated at 473 and 335 cm^{-1} and MnF_2 (orthorhombic) at 469, 413, 386, and 384 cm^{-1} . Experimentally, impurity modes were recorded at least at 482 and 364 cm^{-1} .

Vibrational Spectroscopy on Mn_3F_8

Figure 13 and Figure 14 show a section of the observed IR and Raman spectra of Mn_3F_8 . The complete spectra are shown in Figures S3 and S4. Due to technical issues related to the calculation of IR and Raman intensities for ferrimagnetic materials in CRYSTAL17, it was not possible to calculate IR or Raman spectra for Mn_3F_8 . Even though we cannot make direct comparisons between calculated and experimentally observed spectra, Table 9 shows our band assignment based on visualization of the vibrational modes.

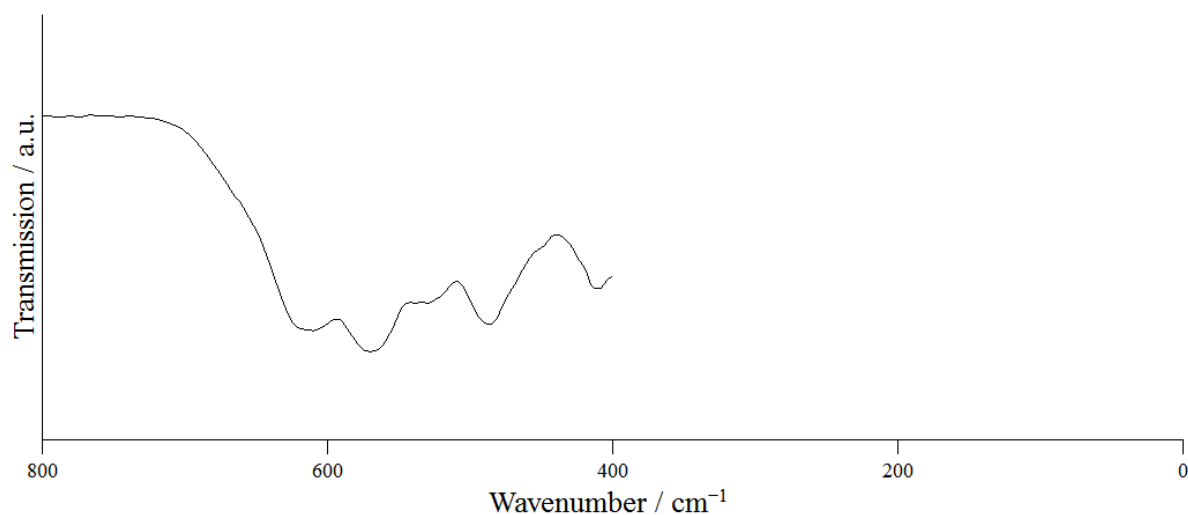


Figure 13. A section of the IR spectrum of Mn_3F_8 . The complete spectrum is given in the SI.

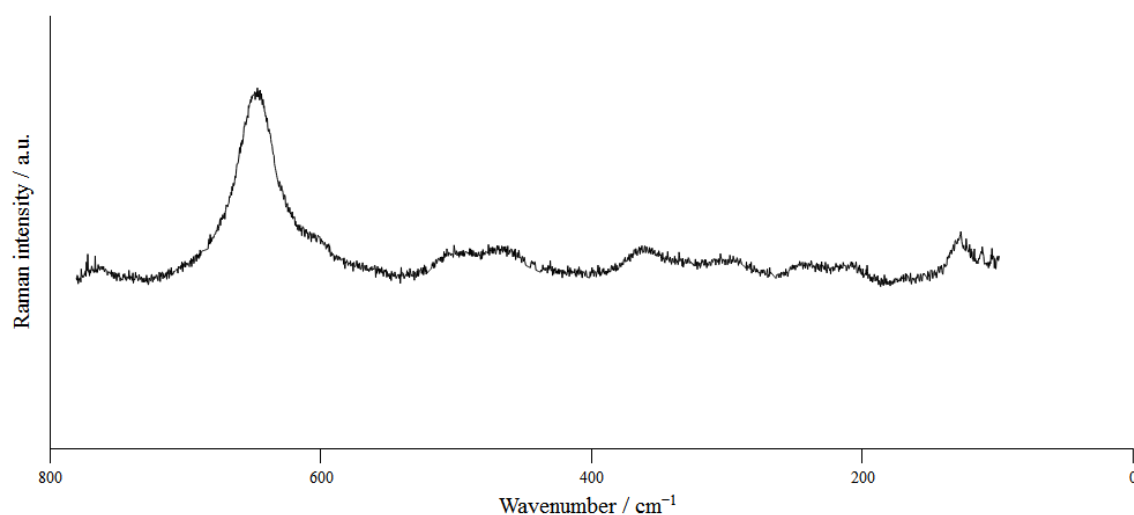


Figure 14. A section of the Raman spectrum of Mn_3F_8 , the complete spectrum is given in the SI.

Table 9. Qualitative assignment of the vibration modes (in cm^{-1}) of Mn_3F_8 .

IR mode	Raman mode	Assignment*
Experiment	Experiment	
	648	Mn(2)–F–Mn(3) and Mn(1)–F–Mn(1) stretching
617		Mn(2)–F–Mn(3) and Mn(1)–F–Mn(1) stretching
	610	Mn(2)–F–Mn(3) and Mn(1)–F–Mn(1) stretching
571		Mn(1)–F–Mn(2) stretching
531		Mn(2)–F–Mn(3) stretching
	502	Mn(1)–F–Mn(2) and Mn(1)–F–Mn(3) stretching
487		Mn(1)–F–Mn(3) stretching
	467	likely MnF_2
410		Mn(1)–F–Mn(2) stretching
	362	Mn–F stretching coupled with bending
	298	Mn–F bending modes
	243	Mn–F bending modes
	212	Mn–F bending modes
	128	lattice vibration

* The bands were assigned by visualizing the normal modes and comparing to the assignment of Mn_2F_5 .

Magnetic Properties of Mn_2F_5

Unfortunately, we could not obtain pure samples of Mn_2F_5 . A Rietveld refinement on the sample used for the magnetic properties' measurement showed a content of circa 6 wt.-% of MnF_2 . We also observed the presence of MnF_2 in the magnetic measurement by a kink in the susceptibility curve at 68 K. Therefore, we only confirm the Néel temperature of Mn_2F_5 and refrain from reporting the effective magnetic moment. The measurements were performed on a sample synthesized within a platinum ampoule (see Experimental Part). We observed the Néel temperature at 53.4 K (Figure 15) in agreement with 54 ± 3 K determined by *Tressaud* and *Dance*.²⁰

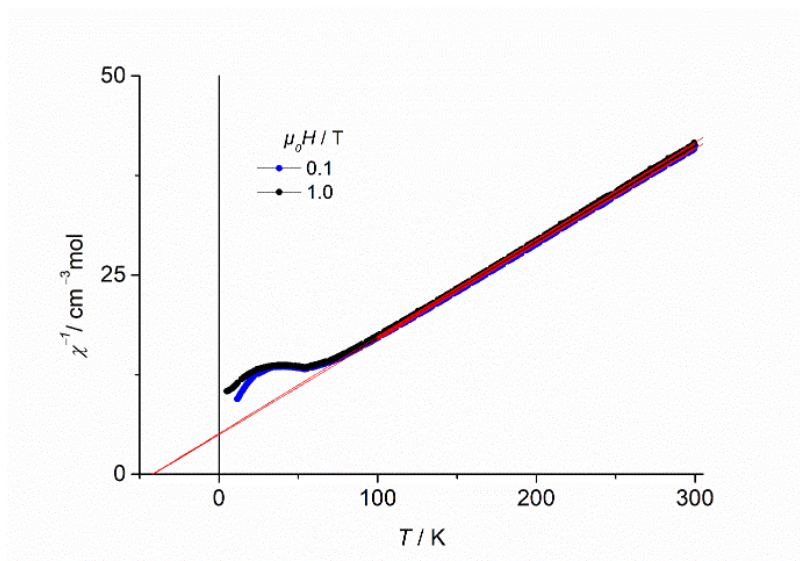


Figure 15. Plot of reciprocal molar susceptibility versus temperature of a sample that mainly contained Mn_2F_5 with some MnF_2 as an impurity.

Magnetic Properties of Mn_3F_8

Our magnetic measurements gave no hints towards impurities within Mn_3F_8 . The measurements were performed on the same sample on which the Le Bail fit (Figure 4) had been carried out. Figure 16 shows a plot of the reciprocal susceptibility of Mn_3F_8 versus the temperature, further plots of molar magnetization and molar susceptibility are available in Figures S5 and S6. The effective magnetic moment was calculated to 9.1 Bohr magnetons (BM, $n_{\text{eff}}^2 = 9.1^2 = 82.8$) per formula unit (see also Figure S7). This corresponds to 5.21 BM for each Mn atom ($3 \cdot 5.21^2 = 81.4$), which agrees with the effective magnetic moment calculated from the spin-only values of two Mn(III) and one Mn(II) centers. $2 \times (4.90 \text{ BM})^2$ for Mn(III) and $1 \times (5.92 \text{ BM})^2$ for Mn(II) is equal to 83.06 which is 9.11^2 .

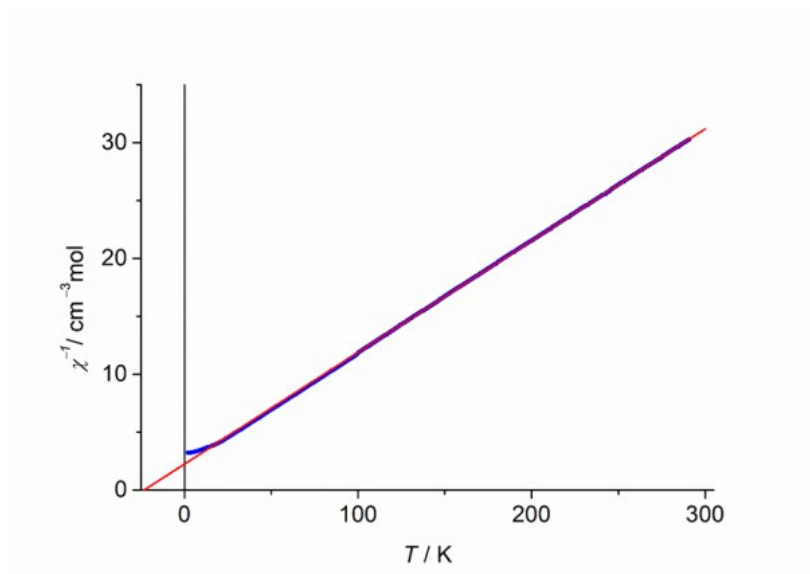


Figure 16. Plot of reciprocal molar susceptibility versus temperature of a sample that mainly contained Mn_3F_8 . A field of 8 T was used. The resulting effective magnetic moment is 9.1 Bohr magnetons (BM) per formula unit, which corresponds to 5.21 BM per manganese atom. The Weiss temperature is -23.2 K.

The Weiss temperature of -23.2 K (Figure 16) indicates an antiferromagnetic/ferrimagnetic behavior for Mn_3F_8 . This can be also seen in Figure S8, where the curve at 20 K has the highest slope. Measurements at low field show a bifurcation of zfc and fc measurements with an additional maximum at 8 K in the zfc curve. This may indicate that a ferromagnetic interaction occurs at low temperatures.

Conclusion

Single crystals of Mn_2F_5 and Mn_3F_8 were obtained performing high-pressure/high-temperature experiments using a multianvil press starting from stoichiometric mixtures of MnF_2 and MnF_3 . Powder X-Ray diffraction analyses as well as IR and Raman spectra showed both bulk compounds to be contaminated with MnF_2 . Quantum chemical calculations allowed for tentative band assignments for both compounds.

Mn_2F_5 crystallizes isotypic to CaCrF_5 in the space group $C2/c$ (no. 15). The Mn(III) atom is coordinated octahedron-like by six fluorine atoms, whereas the Mn(II) atom is coordinated in the shape of a distorted trigonal bipyramid. These two polyhedra are linked with each other and form a three-dimensional infinite network.

To the best of our knowledge, Mn_3F_8 represents a novel structure type. It crystallizes in the space group $P2_1$ (no. 4) with the lattice parameters $a = 5.5253(2)$, $b = 4.8786(2)$, $c =$

9.9124(4) Å, $\beta = 92.608(2)^\circ$, $V = 266.92(2) \text{ \AA}^3$, $Z = 2$, $mP22_1$, $4a^{11}$, at $T = 183 \text{ K}$. The Mn–F distances were also used to assign the oxidation states of the octahedron-like coordinated Mn atoms in this structure. The octahedra are connected with each other and form a three-dimensional infinite network structure. CHARDI calculations and quantum chemical calculations were also performed and verify the assignment of the oxidation states.

Additionally, magnetic data were collected for both compounds but due to the impurity of MnF_2 these data are affected. However, the determined effective magnetic moments of both mixed-valent compounds correspond well with the spin-only values of Mn(II) and Mn(III) atoms.

Experimental Section

Synthesis of Mn_2F_5 inside a platinum ampoule

A platinum ampoule was loaded with a mixture of MnF_2 (187.25 mg, 2.02 mmol) and MnF_3 (229.50 mg, 2.05 mmol) inside a glovebox filled with argon 5.0 (Praxair). This ampoule was sealed via arc welding under 800 mbar argon atmosphere and heated with $1 \text{ }^\circ\text{C}/\text{min}$ inside a tube furnace up to $300 \text{ }^\circ\text{C}$. After 14 days the temperature was decreased with a rate of $0.5 \text{ }^\circ\text{C}/\text{min}$ to room temperature and the ampoule was opened inside a glovebox. This sample was not phase pure either and MnF_2 could be detected by powder X-ray diffraction and Raman spectroscopy as impurity.

Single crystal growth of the title compounds

Single crystals of each compound were obtained using a high-pressure/high-temperature approach. Both experiments were carried out in a 1000 t multianvil press (Max Voggenreiter GmbH, Mainleus, Germany) equipped with a Walker-type module provided by the same company. Stoichiometric amounts of MnF_2 and MnF_3 ($\text{MnF}_2:\text{MnF}_3 = 1:1$ for Mn_2F_5 and $\text{MnF}_2:\text{MnF}_3 = 1:2$ for Mn_3F_8) were weighed inside a glovebox (MBraun Inertgas-System GmbH, Germany) under inert gas atmosphere, thoroughly ground in an agate mortar and transferred into a platinum capsule (99.95%, Ögussa, Vienna, Austria). The capsule was placed into a boron-nitride crucible (Henze Boron Nitride Products AG, Lauben, Germany), which was, in turn, placed into an 18/11 assembly (detailed descriptions of the assembly can be found in literature).^{46–48} A vertical hydraulic ram then compressed the Walker-type module

containing six steel anvils, three facing up and three facing down. The 18/11 assembly surrounded by eight tungsten carbide cubes (Hawedia, Marklkofen, Germany) filled the cavity left by the six steel anvils, completing the setup for a high-pressure/high-temperature experiment using a multianvil press.

For the synthesis of Mn_2F_5 , the sample was compressed to 3.0 GPa within 75 min and kept at that pressure for the rest of the heating program. The sample was heated to 500 °C within 10 min, kept at that temperature for another 30 min and finally cooled to 200 °C within 60 min. The heating was switched off and decompression of the sample back to atmospheric pressure could be realized within 225 min. The platinum capsule was recovered and opened under argon atmosphere, revealing a crystalline sample of pink color (Figure 1).

Mn_3F_8 was synthesized in a very similar manner, adjusting only the pressure acting on the assembly. The sample was compressed to 5.5 GPa within 135 min and kept at that pressure for the entire duration of the subsequent heating program. The sample was heated to 500 °C within 10 min, kept at that temperature for an additional 30 min, then finally cooled down to 200 °C within 60 min. At this point, the heating was switched off entirely and decompression of the sample back to atmospheric pressure was achieved within 415 min. The platinum capsule was recovered and opened under argon atmosphere to reveal a crystalline sample of a strong violet color (Figure 3).

Single crystal X-ray diffraction

A sample of each of the compounds was transferred onto a microscope slide and covered in perfluoralkyl ether to allow observation under a polarization microscope outside of the glovebox. Suitable single crystals were isolated and mounted onto a Bruker D8 Quest single crystal diffractometer (Bruker, Billerica, USA). Using Olex2,⁴⁹ the structures were solved with the SHELXT structure solution program using Intrinsic Phasing⁵⁰ and refined with the SHELXL refinement package⁵¹ using full-matrix Least Squares minimization. All atoms were refined using anisotropic displacement parameters. The y coordinate of the Mn(1) atom of Mn_3F_8 was fixed to zero to save the floating origin restraint. With loose symmetry criteria, the Platon software⁵² detects additional symmetry for the crystal structure of Mn_3F_8 and suggests space group $P2_1/c$. However, a refinement in this space group shows many systematic absence violations of the c glide plane and is therefore not sensible.

CCDC 2089883 (Mn₂F₅) and 2089884 (Mn₃F₈) contain the supplementary crystallographic data for this paper. These data are provided free of charge by [The Cambridge Crystallographic Data Centre](https://www.ccdc.cam.ac.uk/).

Powder X-ray diffraction

The powder X-ray diffraction patterns were recorded at ambient temperature with a Stoe Stadi P powder diffractometer in Debye-Scherrer geometry. The instrument was operated with Mo- $K_{\alpha 1}$ -radiation ($\lambda = 0.7093 \text{ \AA}$, Ge(111) monochromator) and a Mythen 2 DCS4 detector. The evaluations of the powder X-ray patterns were carried out with the WinXPOW 3.07 software package.⁵³ Le-Bail fit (Mn₃F₈) and Rietveld refinement (Mn₂F₅) were performed with Jana2006.⁵⁴ In the course of these refinements, the reflection profiles were fitted with a pseudo-Voigt function. In addition to the profile parameters, a zero-shift parameter was refined. The atom positions and isotropic displacement parameters were fixed. The peak asymmetry for Mn₃F₈ was refined using a divergence correction, for Mn₂F₅ it did not converge, which is why no correction of asymmetry was carried out.

UV/Vis-Spectroscopy

The UV/Vis spectra were measured on a Specord 210 Plus (analytikjena) using a deuterium source for the UV and a halogen lamp for the visual part of the spectrum.

IR spectroscopy

Infrared spectra were measured on a Bruker Alpha Platinum FT-IR spectrometer using the ATR Diamond module with a resolution of 4 cm^{-1} . The spectrometer was located inside a glovebox under argon (5.0, Praxair) atmosphere. For data collection, the OPUS 7.2 software was used.⁵⁵

Raman spectroscopy

The Raman spectrum was recorded with a Confocal Raman Microscope S+I MonoVista CRS+, using the 633 nm excitation line of an integrated diode laser (resolution $< 1 \text{ cm}^{-1}$).⁵⁶ The sample was measured inside a borosilicate glass ampoule.

Magnetic Measurements

DC-magnetic data were collected with the aid of the VSM option of a physical property measurement system (ppms) of Quantum Design.

The collected data were corrected with respect to the diamagnetic moment of the sample holder, as well as to the diamagnetic contribution ($\chi_{\text{dia}} = -1.24 \cdot 10^{-4} \text{ cm}^3 \text{ mol}^{-1}$) of the sample derived from Pascal constants considering the sample mass, the result being the net paramagnetic data.

Quantum Chemical Calculations

Periodic quantum chemical calculations were carried out with the PBE0 hybrid density functional method (DFT-PBE0) using the CRYSTAL17 program package. Gaussian-type triple-zeta-valence + polarization (TZVP) level basis sets were applied for all atoms. The basis sets for Mn and F have been previously derived from the molecular Karlsruhe def2 basis sets.⁵⁷⁻⁵⁹ The following Monkhorst-Pack-type k -meshes were used for sampling the reciprocal space: $8 \times 8 \times 6$ for Mn_2F_5 , $8 \times 8 \times 6$ for Mn_3F_8 , $8 \times 8 \times 12$ for MnF_2 (tetragonal) and $8 \times 6 \times 6$ for MnF_2 (orthorhombic)⁶⁰ For the evaluation of the Coulomb and exchange integrals (TOLINTEG), tight tolerance factors of 8, 8, 8, 8, and 16 were used (very tight factors of 10, 10, 10, 10, and 20 had to be used for IR and Raman spectrum calculation of Mn_2F_5). Default extra-large integration grid was used for the DFT exchange-correlation functional (XLGRID). Both the atomic positions and lattice constants were fully optimized within the constraints imposed by the space group symmetry, using the default optimization convergence criteria of CRYSTAL17. The harmonic vibrational frequencies and IR intensities were obtained by using the computational schemes implemented in CRYSTAL.⁶¹⁻⁶⁴ All optimized structures were confirmed to be true local minima with no imaginary frequencies. The final IR spectra were obtained by using Lorentzian peak profile with FWHM of 16 cm^{-1} . The Raman intensities were calculated for a polycrystalline powder sample (total isotropic intensity in arbitrary units). The Raman spectra were obtained by using a pseudo-Voigt band profile (50:50 Lorentzian:Gaussian) and an FWHM of 8 cm^{-1} . The band assignments were carried out by visual inspection of the normal modes with the Jmol program package.⁶⁵

Acknowledgement

We thank H. L. Deubner for Raman measurements, Dr. M. Conrad for helpful discussions, and Solvay for kind donations of F₂. A. J. K thanks CSC, the Finnish IT Center for Science for computational resources.

Supporting Information

The supporting information contains anisotropic displacement parameters of the crystal structures, the details of the Rietveld refinements, vibrational spectra, magnetic measurements, and quantum-chemical calculations.

References

- (1) Berzelius, J. J. Untersuchungen über die Flussspathsäure und deren merkwürdigsten Verbindungen. *Ann. Phys. (Berlin, Ger.)* **1824**, *77* (5), 1–48. <https://doi.org/10.1002/andp.18240770502>.
- (2) van Arkel, A. E. Über die Kristallstruktur der Verbindungen Manganfluorid, Bleijodid und Wolframsulfid. *Recl. Trav. Chim. Pays-Bas* **1926**, *45* (6), 437–444. <https://doi.org/10.1002/recl.19260450612>.
- (3) Nicklès, J. Sur de Nouvelles Combinaisons Manganiques. *C. R. Hebd. Seances Acad. Sci.* **1867**, *65*, 107–111.
- (4) Moissan, H. Préparation et Propriétés D'un Perfluorure de Manganèse. *C. R. Hebd. Seances Acad. Sci.* **1900**, *130*, 622–627.
- (5) von Wartenberg, H. Über Einige Höhere Fluoride (PbF₄, CeF₄, BiF₅). *Z. Anorg. Allg. Chem.* **1940**, *244* (4), 337–347. <https://doi.org/10.1002/zaac.19402440401>.
- (6) Georg Brauer. *Handbuch der präparativen anorganischen Chemie*, 3rd ed.; Ferdinand Enke Verlag: Stuttgart, 1975.
- (7) Mazej, Z. Room Temperature Syntheses of MnF₃, MnF₄ and Hexafluoromanganate(IV) Salts of Alkali Cations. *J. Fluorine Chem.* **2002**, *114*, 75–80.
- (8) Hepworth, M. A.; Jack, K. H. The Crystal Structure of Manganese Trifluoride MnF₃. *Acta Crystallogr.* **1957**, *10*, 345–351.
- (9) Hepworth, M. A.; Jack, K. H. Interatomic Bonding in Manganese Trifluoride. *Nature* **1957**, 211–212.
- (10) Schrötter, F.; Müller, B. G. Zur Kristallstruktur von MnF₃ und MnPtF₆. *Z. Anorg. Allg. Chem.* **1993**, *619* (8), 1426–1430. <https://doi.org/10.1002/zaac.19936190818>.
- (11) Bandemehr, J.; Stoll, C.; Heymann, G.; Ivlev, S. I.; Karttunen, A. J.; Conrad, M.; Huppertz, H.; Kraus, F. The Crystal Structure of MnF₃ Revisited. *Z. Anorg. Allg. Chem.* **2020**, *646*, 882–888. <https://doi.org/10.1002/zaac.202000025>.
- (12) Hoppe, R.; Dähne, W.; Klemm, W. Mangantetrafluorid, MnF₄. *Naturwissenschaften* **1961**, *48*, 429–429.
- (13) Hoppe, R.; Dähne, W.; Klemm, W. Mangantetrafluorid Mit Einem Anhang Über LiMnF₅ Und LiMnF₄. *Liebigs Ann. Chem.* **1962**, *658*, 1–5.

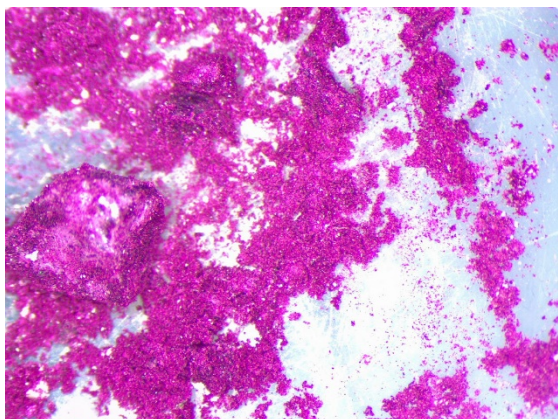
- (14) Roesky, H.; Glemser, O. Neue Darstellung von Mangantetrafluorid. *Angew. Chem.* **1963**, *75* (19), 920–921. <https://doi.org/10.1002/ange.19630751914>.
- (15) Court, T. L.; Dove, M. F. A. Reactions of Complex Fluorides of Some 3d Metals in Anhydrous Hydrogen Fluoride. *J. Chem. Soc. D* **1971**, No. 14, 726–726. <https://doi.org/10.1039/C29710000726>.
- (16) Lutar, K.; Jesih, A.; Žemva, B. KrF₂/MnF₄ Adducts from KrF₂/MnF₂ Interaction in HF as a Route to High Purity MnF₄. *Polyhedron* **1988**, *7* (13), 1217–1219. [https://doi.org/10.1016/S0277-5387\(00\)81212-7](https://doi.org/10.1016/S0277-5387(00)81212-7).
- (17) Müller, B. G.; Serafin, M. Die Kristallstruktur von Mangantetrafluorid. *Z. Naturforsch., B: J. Chem. Sci.* **1987**, *42*, 1102–1106.
- (18) Kraus, F.; Ivlev, S. I.; Bandemehr, J.; Sachs, M.; Pietzonka, C.; Conrad, M.; Serafin, M.; Müller, B. G. Synthesis and Characterization of Manganese Tetrafluoride β -MnF₄. *Z. Anorg. Allg. Chem.* **2020**, *646*, 1481–1489. <https://doi.org/10.1002/zaac.202000048>.
- (19) Ehlert, T. C.; Hsia, M. Mass Spectrometric and Thermochemical Studies of the Manganese Fluorides. *J. Fluorine Chem.* **1972**, *2* (1), 33–51. [https://doi.org/10.1016/S0022-1139\(00\)83113-9](https://doi.org/10.1016/S0022-1139(00)83113-9).
- (20) Tressaud, A.; Dance, J.-M. Mn₂F₅. *C. R. Acad. Sc. Paris* **1974**, *278*, 463–465.
- (21) Férey, G.; Leblanc, M.; Jacoboni, C.; De Pape, R. Sur Le Fluorure Double MnCrF₅. *C. R. Acad. Sc. Paris* **1971**, *273*, 700–702.
- (22) Férey, G.; de Pape, R.; Boucher, B. Structure magnétique du fluorure antiferromagnétique MnCrF₅. *Acta Crystallogr., Sect. B: Struct. Crystallogr. Cryst. Chem.* **1978**, *34* (4), 1084–1091. <https://doi.org/10.1107/S0567740878004975>.
- (23) Rau, J. V.; Albertini, V. R.; Chilingarov, N. S.; Colonna, S.; Tamburini, U. A. In Situ Time-Resolved X-Ray Diffraction Study of Manganese Trifluoride Thermal Decomposition. *J. Fluorine Chem.* **2001**, *108* (2), 253–256. [https://doi.org/10.1016/S0022-1139\(01\)00368-2](https://doi.org/10.1016/S0022-1139(01)00368-2).
- (24) Rau, J. V.; Rossi Albertini, V.; Chilingarov, N. S.; Di Michiel, M.; Colonna, S.; Ioffe, I. N.; Sidorov, L. N. In Situ Very-High-Energy Diffraction Studies of Thermal Decomposition of Transition Metal Trifluorides. *Bull. Chem. Soc. Jpn.* **2003**, *76* (6), 1165–1169. <https://doi.org/10.1246/bcsj.76.1165>.
- (25) Wandner, K.-H.; Hoppe, R. Zum Jahn-Teller-Effekt Bei Mn(III)-Fluoriden: CaMnF₆. *Rev. Chim. Miner.* **1986**, *23*, 520–531.
- (26) Wandner, K.-H.; Hoppe, R. Die Kristallstruktur von CdMnF₅. *Z. Anorg. Allg. Chem.* **1988**, *557*, 153–160.
- (27) Wu, K. K.; Brown, I. D. Refinement of the Crystal Structure of CaCrF₅. *Mater. Res. Bull.* **1973**, *8* (5), 593–598. [https://doi.org/10.1016/0025-5408\(73\)90137-2](https://doi.org/10.1016/0025-5408(73)90137-2).
- (28) Müller, U.; Hoppe, R. Korrektur zu den Kristallstrukturen von CaMnF₅ und CdMnF₅. *Z. Anorg. Allg. Chem.* **1990**, *583* (1), 205–208. <https://doi.org/10.1002/zaac.19905830125>.
- (29) Stoll, C.; Atanasov, M.; Bandemehr, J.; Neese, F.; Pietzonka, C.; Kraus, F.; Karttunen, A. J.; Seibald, M.; Heymann, G.; Huppertz, H. Coexistence of Two Different Distorted Octahedral [MnF₆]³⁻ Sites in K₃[MnF₆]: Manifestation in Spectroscopy and Magnetism. *Chem. Eur. J.* No. <https://doi.org/10.1002/chem.202005496>. <https://doi.org/10.1002/chem.202005496>.

- (30) English, U.; Massa, W.; Tressaud, A. Structure of Trisodium Hexafluoromanganate(III). *Acta Crystallogr., Sect. C: Cryst. Struct. Commun.* **1992**, *48* (1), 6–8. <https://doi.org/10.1107/S0108270191009071>.
- (31) Jensen, W. B. Chapter II - Crystal Coordination Formulas: A Flexible Notation for the Interpretation of Solid-State Structures. In *Cohesion and Structure*; Hafner, J., Hulliger, F., Jensen, W. B., Majewski, J. A., Mathis, K., Villars, P., Vogl, P., Eds.; The Structures of Binary Compounds; North-Holland, 1989; Vol. 2, pp 105–146. <https://doi.org/10.1016/B978-0-444-87478-8.50006-2>.
- (32) Hoppe, R. Über Madelungfaktoren. *Angew. Chem.* **1966**, *78* (1), 52–63.
- (33) Hoppe, R. Die Koordinationszahl — ein „anorganisches Chamäleon“. *Angew. Chem.* **1970**, *82* (1), 7–16. <https://doi.org/10.1002/ange.19700820103>.
- (34) Hübenenthal, R. *MAPLE Version 4.0*; Gießen, 1993.
- (35) Brown, I. D.; Altermatt, D. Bond-Valence Parameters Obtained from a Systematic Analysis of the Inorganic Crystal Structure Database. *Acta Crystallogr., Sect. B: Struct. Sci.* **1985**, *41*, 244–247. <https://doi.org/doi.org/10.1107/S0108768185002063>.
- (36) Brese, N. E.; O’Keeffe, M. Bond-Valence Parameters for Solids. *Acta Crystallogr., Sect. B: Struct. Sci.* **1991**, *47* (2), 192–197. <https://doi.org/10.1107/S0108768190011041>.
- (37) Hoppe, R. Effective Coordination Numbers (ECoN) and Mean Fictive Ionic Radii (MEFIR). *Z. Kristallogr. - Cryst. Mater.* **1979**, *150* (1–4), 23–52.
- (38) Hoppe, R.; Voigt, S.; Glaum, H.; Kissel, J.; Müller, H. P.; Bernet, K. A New Route to Charge Distributions in Ionic Solids. *J. Less-Common Met.* **1989**, *156* (1), 105–122. [https://doi.org/10.1016/0022-5088\(89\)90411-6](https://doi.org/10.1016/0022-5088(89)90411-6).
- (39) Férey, G.; De Pape, R.; Poulain, M.; Grandjean, D.; Hardy, A. La Structure Cristalline de MnCrF₅. *Acta Crystallogr., Sect. B: Struct. Crystallogr. Cryst. Chem* **1977**, *33*, 1409–1413. <https://doi.org/doi.org/10.1107/S0567740877006189> share.
- (40) Dumora, D.; Von der Mühl, R.; Ravez, J. Structure Cristalline de CaCrF₅. *Mater. Res. Bull.* **1971**, *6* (7), 561–569. [https://doi.org/10.1016/0025-5408\(71\)90005-5](https://doi.org/10.1016/0025-5408(71)90005-5).
- (41) Baur, W. H.; Khan, A. A. Rutile-Type Compounds. IV. SiO₂, GeO₂ and a Comparison with Other Rutile-Type Structures. *Acta Crystallogr., Sect. B: Struct. Crystallogr. Cryst. Chem.* **1971**, *27*, 2133–2139. <https://doi.org/doi.org/10.1107/S0567740871005466>.
- (42) Baur, W. H. Über Die Verfeinerung Der Kristallstrukturbestimmung Einiger Vertreter Des Rutiltyps. II. Die Difluoride von Mn, Fe, Co, Ni Und Zn. *Acta Crystallogr.* **1958**, *11*, 488–490.
- (43) Kabalkina, S. S.; Popova, S. V. Phase Transition in Zinc and Manganese Fluorides at High Pressures and High Temperatures., *Dokl. Akad. Nauk SSSR* **1963**, *153* (6), 1310–1312.
- (44) Golosovsky, I. V.; Sokolov, N. S.; Kaveev, A. K.; Boehm, M.; Nogués, J.; Nannarone, S. Magnetic Order in an MnF₂ Epitaxial Layer with the Orthorhombic Structure. *Jetp Lett.* **2006**, *83* (4), 152–155. <https://doi.org/10.1134/S0021364006040059>.
- (45) Kabalkina, S. S.; Vereshchagin, L. F.; Lityagina, L. M. POLYMORPHISM OF MnF₂ AT HIGH PRESSURES AND TEMPERATURES. *Sov. Phys. JETP* **1969**, *29* (5), 803–806.

- (46) Walker, D.; Carpenter, M. A.; Hitch, C. M. Some Simplifications to Multianvil Devices for High Pressure Experiments. *Am. Mineral.* **1990**, *75* (9–10), 1020–1028.
- (47) Walker, D. Lubrication, Gasketing, and Precision in Multianvil Experiments. *Am. Mineral.* **1991**, *76* (7–8), 1092–1100.
- (48) Huppertz, H. Multianvil High-Pressure / High-Temperature Synthesis in Solid State Chemistry. *Z. Kristallogr. - Cryst. Mater.* **2004**, *219* (6), 330–338. <https://doi.org/10.1524/zkri.219.6.330.34633>.
- (49) Dolomanov, O. V.; Bourhis, L. J.; Gildea, R. J.; Howard, J. A. K.; Puschmann, H. *OLEX2*: A Complete Structure Solution, Refinement and Analysis Program. *J. Appl. Crystallogr.* **2009**, *42* (2), 339–341. <https://doi.org/10.1107/S0021889808042726>.
- (50) Sheldrick, G. M. SHELXT – Integrated Space-Group and Crystal-Structure Determination. *Acta Crystallogr., Sect. A: Found. Adv.* **2015**, *71* (1), 3–8. <https://doi.org/10.1107/S2053273314026370>.
- (51) Sheldrick, G. M. Crystal Structure Refinement with *SHELXL*. *Acta Crystallogr., Sect. C: Struct. Chem.* **2015**, *71* (1), 3–8. <https://doi.org/10.1107/S2053229614024218>.
- (52) Spek, A. L. Structure Validation in Chemical Crystallography. *Acta Crystallogr., Sect. D: Biol. Crystallogr.* **2009**, *65* (2), 148–155. <https://doi.org/10.1107/S090744490804362X>.
- (53) *STOE WinXPOW*; STOE & Cie GmbH: Darmstadt, Germany, 2015.
- (54) Petříček, V.; Dušek, M.; Palatinus, L. Crystallographic Computing System JANA2006: General Features. *Z. Kristallogr. - Cryst. Mater.* **2014**, *229* (5), 345–352. <https://doi.org/10.1515/zkri-2014-1737>.
- (55) *OPUS V7.2*; Bruker Optik GmbH: Ettlingen, Germany, 2012.
- (56) *VistaControl*; Spectroscopy and Imaging GmbH: Warstein, Germany, 2018.
- (57) Weigend, F.; Ahlrichs, R. Balanced Basis Sets of Split Valence, Triple Zeta Valence and Quadruple Zeta Valence Quality for H to Rn: Design and Assessment of Accuracy. *Phys. Chem. Chem. Phys.* **2005**, *7* (18), 3297–3305. <https://doi.org/10.1039/B508541A>.
- (58) Linnera, J.; Karttunen, A. J. Lattice Dynamical Properties of Antiferromagnetic MnO, CoO, and NiO, and the Lattice Thermal Conductivity of NiO. *Phys. Rev. B* **2019**, *100* (14), 144307. <https://doi.org/10.1103/PhysRevB.100.144307>.
- (59) Karttunen, A. J.; Tynell, T.; Karppinen, M. Atomic-Level Structural and Electronic Properties of Hybrid Inorganic–Organic ZnO:Hydroquinone Superlattices Fabricated by ALD/MLD. *J. Phys. Chem. C* **2015**, *119* (23), 13105–13114. <https://doi.org/10.1021/acs.jpcc.5b03433>.
- (60) Monkhorst, H. J.; Pack, J. D. Special Points for Brillouin-Zone Integrations. *Phys. Rev. B* **1976**, *13* (12), 5188–5192. <https://doi.org/10.1103/PhysRevB.13.5188>.
- (61) Pascale, F.; Zicovich-Wilson, C. M.; López Gejo, F.; Civalleri, B.; Orlando, R.; Dovesi, R. The Calculation of the Vibrational Frequencies of Crystalline Compounds and Its Implementation in the CRYSTAL Code. *J. Comput. Chem.* **2004**, *25* (6), 888–897. <https://doi.org/10.1002/jcc.20019>.
- (62) Zicovich-Wilson, C. M.; Pascale, F.; Roetti, C.; Saunders, V. R.; Orlando, R.; Dovesi, R. Calculation of the Vibration Frequencies of Alpha-Quartz: The Effect of Hamiltonian and Basis Set. *J. Comput. Chem.* **2004**, *25* (15), 1873–1881. <https://doi.org/10.1002/jcc.20120>.

- (63) Maschio, L.; Kirtman, B.; Orlando, R.; R  rat, M. Ab Initio Analytical Infrared Intensities for Periodic Systems through a Coupled Perturbed Hartree-Fock/Kohn-Sham Method. *J. Chem. Phys.* **2012**, *137* (20), 204113. <https://doi.org/10.1063/1.4767438>.
- (64) Maschio, L.; Kirtman, B.; R  rat, M.; Orlando, R.; Dovesi, R. Ab Initio Analytical Raman Intensities for Periodic Systems through a Coupled Perturbed Hartree-Fock/Kohn-Sham Method in an Atomic Orbital Basis. I. Theory. *J. Chem. Phys.* **2013**, *139* (16), 164101. <https://doi.org/10.1063/1.4824442>.
- (65) *Jmol: an open-source Java viewer for chemical structures in 3D*. <http://www.jmol.org/>; Jmol Team, 2019.

For Table of Contents Only



Single crystals of the binary mixed-valent fluorides Mn₂F₅ and Mn₃F₈ were obtained using a high-pressure/high-temperature approach. Mn₂F₅ crystallizes isotypic to CaCrF₅ in the monoclinic space group $C2/c$ while Mn₃F₈ crystallizes in the non-centrosymmetric monoclinic space group $P2_1$ and presents a new structure type. Photo of a sample of Mn₃F₈ containing small amounts of pale pink MnF₂ as a side phase under an optical microscope.